Analyses and simulations of the upper ocean's response to Hurricane Felix at the Bermuda Testbed Mooring site: 13–23 August 1995

S. E. Zedler,[1] T. D. Dickey,[1] S. C. Doney,[2] J. F. Price,[3] X. Yu,[1] and G. L. Mellor[4]

Received 14 May 2001; revised 22 January 2002; accepted 19 April 2002; published 26 December 2002.

[1] The center of Hurricane Felix passed 85 km to the southwest of the Bermuda Testbed Mooring (BTM; 31°44′N, 64°10′W) site on 15 August 1995. Data collected in the upper ocean from the BTM during this encounter provide a rare opportunity to investigate the physical processes that occur in a hurricane's wake. Data analyses indicate that the storm caused a large increase in kinetic energy at near-inertial frequencies, internal gravity waves in the thermocline, and inertial pumping, mixed layer deepening, and significant vertical redistribution of heat, with cooling of the upper 30 m and warming at depths of 30–70 m. The temperature evolution was simulated using four one-dimensional mixed layer models: Price-Weller-Pinkel (PWP), K Profile Parameterization (KPP), Mellor-Yamada 2.5 (MY), and a modified version of MY2.5 (MY2). The primary differences in the model results were in their simulations of temperature evolution. In particular, when forced using a drag coefficient that had a linear dependence on wind speed, the KPP model predicted sea surface cooling, mixed layer currents, and the maximum depth of cooling closer to the observations than any of the other models. This was shown to be partly because of a special parameterization for gradient Richardson number (R_{gKPP}) shear instability mixing in response to resolved shear in the interior. The MY2 model predicted more sea surface cooling and greater depth penetration of kinetic energy than the MY model. In the MY2 model the dissipation rate of turbulent kinetic energy is parameterized as a function of a locally defined Richardson number (R_{gMY2}) allowing for a reduction in dissipation rate for stable Richardson numbers (R_{gMY2}) when internal gravity waves are likely to be present. Sensitivity simulations with the PWP model, which has specifically defined mixing procedures, show that most of the heat lost from the upper layer was due to entrainment (parameterized as a function of bulk Richardson number R_{bPWP}), with the remainder due to local Richardson number (R_{gPWP}) instabilities. With the exception of the MY model the models predicted reasonable estimates of the north and east current components during and after the hurricane passage at 25 and 45 m. Although the results emphasize differences between the modeled responses to a given wind stress, current controversy over the formulation of wind stress from wind speed measurements (including possible sea state and wave age and sheltering effects) cautions against using our results for assessing model skill. In particular, sensitivity studies show that MY2 simulations of the temperature evolution are excellent when the wind stress is increased, albeit with currents that are larger than observed. Sensitivity experiments also indicate that preexisting inertial motion modulated the amplitude of poststorm currents, but that there was probably not a significant resonant response because of clockwise wind rotation for our study site. *INDEX TERMS:* 4504 Oceanography: Physical: Air/sea interactions (0312); 4572 Oceanography: Physical: Upper ocean processes; 4255 Oceanography: General: Numerical modeling; 4544 Oceanography: Physical: Internal and inertial waves; *KEYWORDS:* hurricane, tropical cyclone, mixed layer modeling, upper ocean processes, inertial currents, ocean storms

Citation: Zedler, S. E., T. D. Dickey, S. C. Doney, J. F. Price, X. Yu, and G. L. Mellor, Analyses and simulations of the upper ocean's response to Hurricane Felix at the Bermuda Testbed Mooring site: 13–23 August 1995, *J. Geophys. Res.*, *107*(C12), 3232, doi:10.1029/2001JC000969, 2002.

[1]Ocean Physics Laboratory, University of Cailfornia, Santa Barbara, Santa Barbara, California, USA.
[2]National Center for Atmospheric Research, Boulder, Colorado, USA.
[3]Woods Hole Oceanographic Institution, Woods Hole, Massachusetts, USA.
[4]Princeton University, Princeton, New Jersey, USA.

0148-0227/02/2001JC000969$09.00

1. Introduction

[2] A classical problem of physical oceanography concerns the upper ocean's response to extreme wind-forcing by a moving storm or hurricane [e.g., *Price*, 1981, 1983; *Greatbatch*, 1983; *Gill*, 1984; *Price et al.*, 1994] (see *Ginis* [1995] for a comprehensive review). The difficulty of making shipboard measurements under such extreme con-

ditions and the sparseness of moored instrumentation has largely limited investigations of posthurricane dynamics to theoretical and modeling studies. However, a few existing data sets are appropriate for comparative modeling studies [e.g., *Brooks*, 1983; *Sanford et al.*, 1987; *Shay and Elsberry*, 1987; *Brink*, 1989; *Dickey et al.*, 1998a, 1998b, 2001; *Zedler*, 1999]. The limited number of hurricane wake data sets have been collected almost exclusively from moorings in shallow coastal waters where tides, shallow water waves, and topographic and bottom boundary effects complicate the evolution of the mixed layer and thus data interpretation and modeling [e.g., *Dickey et al.*, 1998b; *Souza et al.*, 2001]. Modeling and theoretical studies of the upper ocean response to strong impulsive wind-forcing have usually focused on the open ocean. To our knowledge, Hurricane Gloria [*Brink*, 1989] is the only other documented case of mooring time series observations (e.g., temperature and currents) of hurricane passage over deep waters aside from Hurricane Felix [*Dickey et al.*, 1998a, 2001].

[3] The Bermuda Testbed Mooring (BTM) Hurricane Felix data set presents a unique opportunity to study upper ocean response to a passing hurricane in the open ocean. Several of the expected upper ocean responses to a hurricane were observed. These include a large decrease in sea surface temperature (SST), strong inertial motion, generation of large amplitude internal gravity waves in the thermocline, strong vertical turbulent mixing and heat exchange, and cooling of the upper mixed layer that persisted for several days. The work of *Dickey et al.* [1998a], which described the general observations of Hurricane Felix and presented scaling arguments, is expanded here through more detailed analyses and modeling of these responses. Additionally, this data set is used to evaluate the capability of one-dimensional models to simulate the temperature and current responses observed at the BTM site under conditions of a strong, impulsive wind. The mixed layer models are also used to examine the importance of various physical processes, to predict the effects of preexisting near-inertial currents on poststorm dynamics, and to study the effect of hypothetical clockwise and anticlockwise wind rotation during the hurricane (at near-inertial frequencies) on the simulated current response. Other highly important issues involve the calculation of wind stress from hurricane force wind speed measurements from a buoy. Specifically this could entail the possible presence of young waves [*Donelan et al.*, 1993, 1995], the presence of cross-wind or counterwind swell [*Donelan et al.*, 1997], and wave sheltering effects [*Large et al.*, 1995]. At high wind speeds, the parameterization of wind stress is highly controversial. For example, two different studies offer drag coefficients that vary by a factor of about 2 for wind speeds of 25 m/s under conditions of a fully developed sea [*Donelan et al.*, 1995].

[4] The paper is organized as follows. Section 2 introduces the sampling sites used for data collection. Sections 3 and 4 describe conditions prior to and after the passage of Hurricane Felix, respectively. In Section 5 the construction of the surface forcing data set and initial conditions are discussed. Section 6 briefly outlines the models used for the study. Results from sensitivity experiments using, and discussion of, the numerical simulation experiments are presented in sections 7, 8, and 9, respectively. The conclusions are summarized in section 10. The notation section contains a list of variables and values of empirical constants. Details concerning the calculations made for this paper and construction of the surface wind-forcing and heat flux data sets are provided in Appendices A and B, respectively.

2. Sampling Sites

[5] Data used for this study were collected from four sampling sites off the coast of Bermuda (Figure 1a). Time series of surface wind speed and insolation, and subsurface variables at various depths were collected at the Bermuda Testbed Mooring site. Measurements of temperature and horizontal current components were made at 25, 45, 71, and 106 m depths using multivariable moored systems (MVMS; for currents, temperature, conductivity, and bio-optical properties; [*Dickey et al.*, 1998c]) and S4 (for currents and temperature) instrument packages (Figure 1b). Additional temperature sensors were located at depths of 60, 120, and 150 m. Temperature and salinity profiles on 10 August were taken at the Hydrostation S site [*Michaels and Knap*, 1996], which is located 60 km from the BTM site in ~2000 m of water. Temperature profiles from 18 August were taken from the Bermuda Atlantic Time Series (BATS) [*Steinberg et al.*, 2001], and the Bermuda Bio-Optics Program (BBOP) [*Siegel et al.*, 2001] sampling sites, which are near the BTM site.

3. Conditions at BTM Mooring Site Prior to Hurricane Passage

[6] Prior to the passage of Hurricane Felix (on 15 August 1995), wind speed and gust measured at 4.2 m height above the sea surface were less than ~12 m/s (23 kt) as indicated in Figure 2c. Sea surface temperature (SST) was generally spatially uniform (<0.5°C different from 29°C) within a 100 km radius of the BTM (based on AVHRR SST imagery [*Nelson*, 1996]) and was increasing (Figure 2a). Stratification of the upper layer was also increasing (Figure 2). The vertical spacing of the temperature sensors was too coarse to precisely resolve the mixed layer depth (defined here as the depth where the temperature is 0.5°C cooler than near sea surface temperature), but profile measurements indicate that on 10 August, it was ~20 m at Hydrostation S (Figure 3). Importantly, Hydrostation S temperatures in the upper 100 m of water were within the uncertainty of the BTM measurements for this date, suggesting that there was likely little spatial difference in upper ocean temperature between the two sites (typically maximum of 1.2°C in summer [*Michaels and Knap*, 1996]). Variability in temperature at 25 m (prior to the storm) and at 45 m (subsequent to the passage of Hurricane Felix; Figure 2b) suggests that the sensors at these depths were at times alternately in the mixed layer and the upper portion of the thermocline before and after the storm passage, respectively. Near-inertial currents of amplitude 20 cm/s were observed at 25 m prior to passage of Hurricane Felix (e.g., during 12–15 August; Figure 2e); these likely affected the upper ocean's response to the hurricane and poststorm dynamics. The effect of preexisting currents on poststorm current strength is assessed using the MY2 and KPP models in section 8 of this paper. Near-inertial current amplitudes generally decreased with depth. Time series of current and temperature records at 106 m (which appear to be of good quality) may be offset in time because the sensors at that depth appear to have ceased recording data for an uncertain period (likely no more than a day) between late

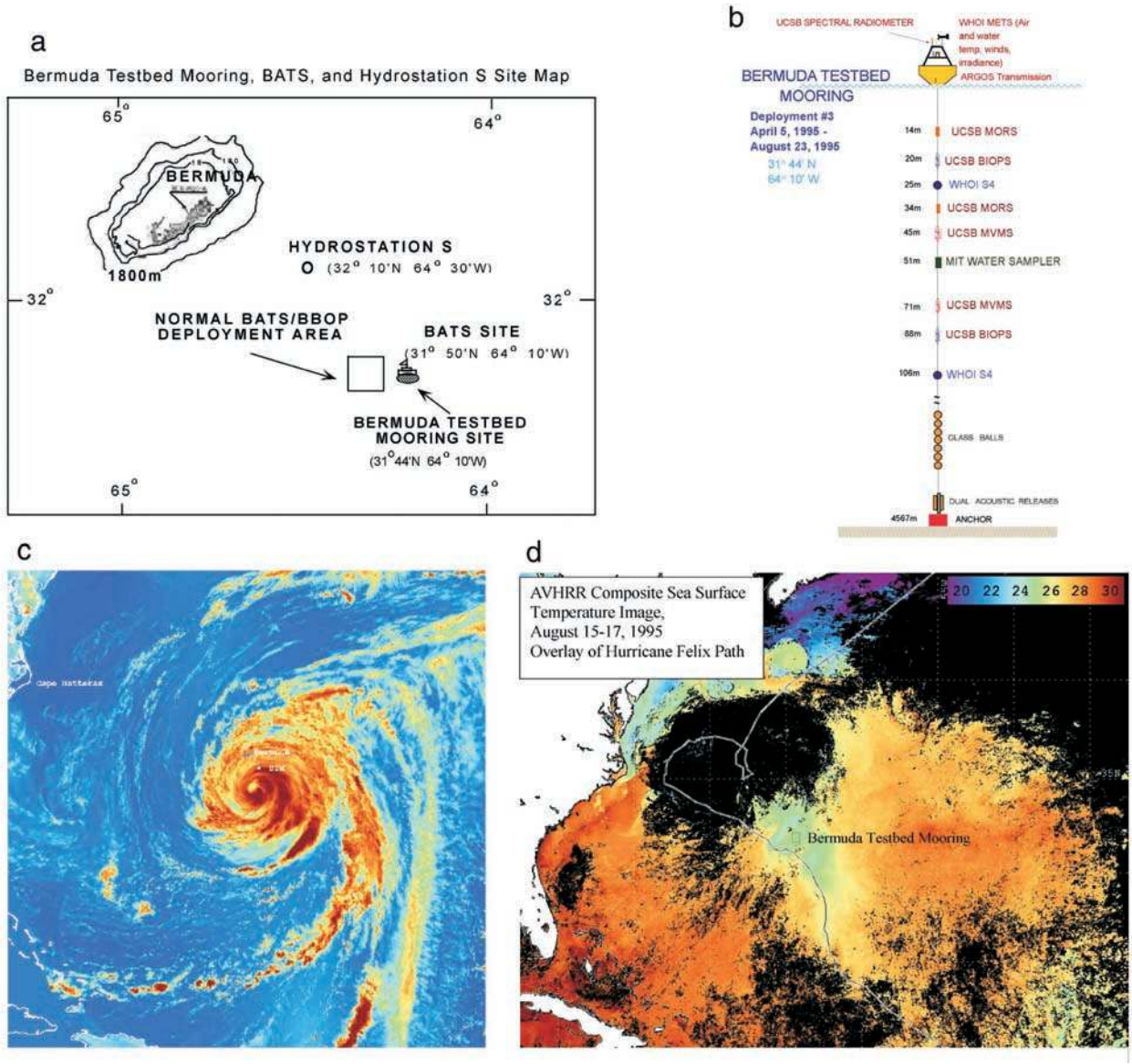

Figure 1. (a) Map showing location of Hydrostation S, BATS/BBOP, and BTM sampling sites relative to Bermuda. (b) Mooring diagram for the BTM showing depths of various instrument packages that were deployed during the passage of Hurricane Felix. (c) False color satellite image showing cloud structure of Hurricane Felix, provided courtesy of N. Nelson. (d) Three-day composite AVHRR sea surface temperature image for the time interval 15–17 August 1995, with overlay of hurricane track [*Nelson*, 1996]. Note the cool swath of water to the right of the hurricane track.

July and early August. The strong near-inertial component of motion near the end of the record was used to approximate the time shift between the 106 m data and data collected at other depths (Figure 2).

4. Atmospheric Forcing and Observed Response to Felix

[7] The center of Hurricane Felix passed 85 km to the southwest of the BTM site on 15 August 1995. The eyewall (northeast sector) passed almost directly over the mooring according to satellite imagery (Figure 1) [*Nelson*, 1996]). Between midnight and noon of 14 August, average wind speed and wind gust (both measured at 4.2 m height above the sea surface) rose steadily to values greater than 20 m/s (39 kt) and 27 m/s (52 kt), respectively, and persisted for about 14 hours (Figure 2c). Average winds declined steadily except for a period of a few days (~19–21 August) after the hurricane passage.

4.1. Temperature Response

[8] Hurricane Felix interrupted trends of heating and increasing stratification of the upper layer of the ocean (Figure 2a), causing extensive vertical mixing characterized by prolonged cooling of the upper 30 m, deepening of the mixed layer, and heating from depths of ~30–70 m (Figures 1, 2, and 3). These effects can be attributed to a combination of mixing in the thermocline, entrainment of

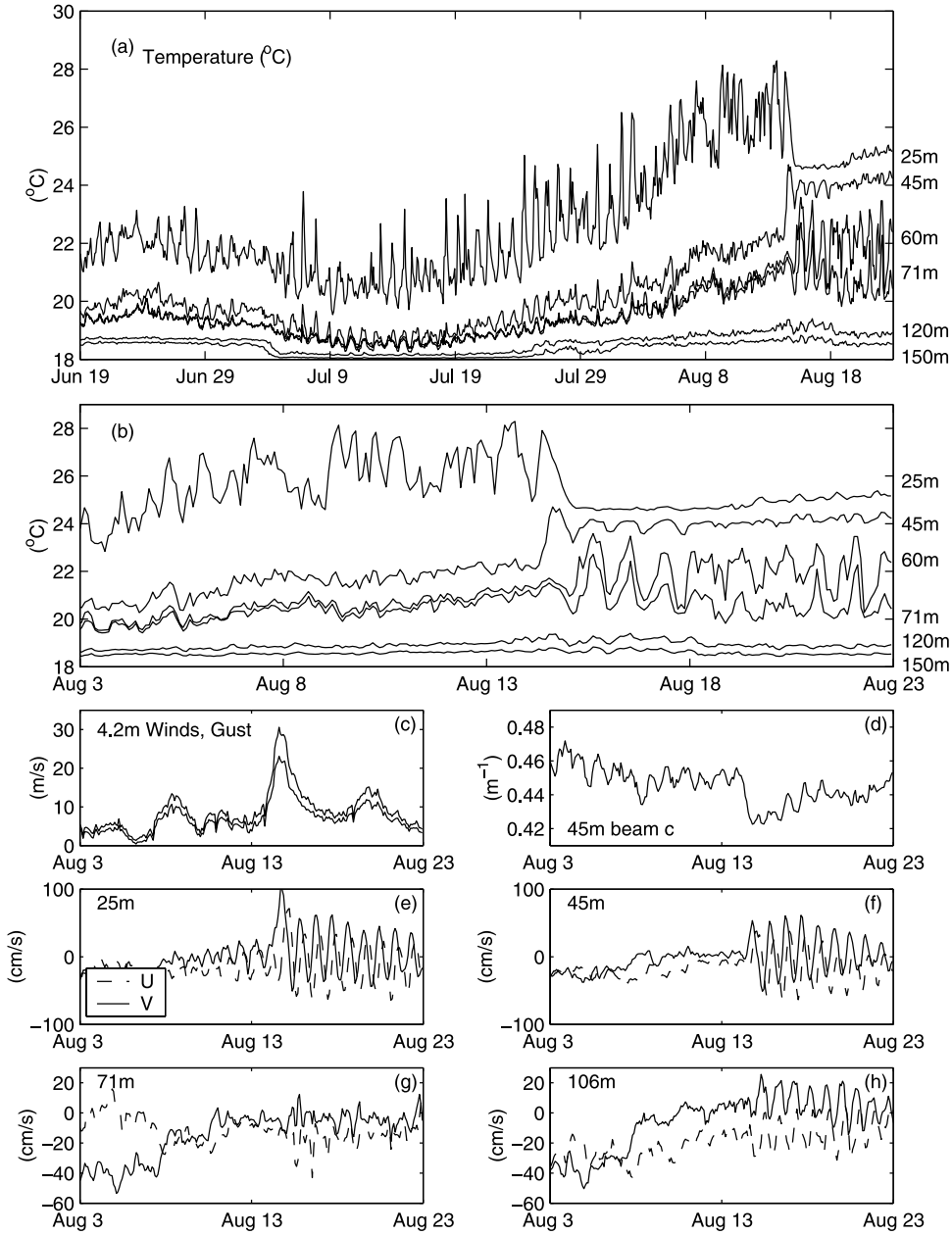

Figure 2

Figure 2. All measurements shown in Figure 2 were made using the BTM. (a) Time series of temperature (°C) at depths of 25, 45, 60, 71, 120, and 150 m (top to bottom) from 19 June to 23 August. Prior to Hurricane Felix, conditions at the BTM site were typical for midsummer, and the ocean was undergoing strong heating and stratification. After the passage of Felix the upper mixed layer cooled by 3.0°–3.5°C. Warming and inertial pumping was evident in the thermocline (45 and 60 m records, respectively). (b) Enlargement of Figure 2a for 3–23 August. (c) Time series of wind speed and wind gust (both in m/s), showing hurricane force winds on 15 August. (d) Time series of beam c at 45 m. Measured north (V) and east (U) current components at a specific depth in units of cm/s: (e) 25, (f) 45, (g) 71, and (h) 106 m.

cooler water at the base of the mixed layer, and heat loss at the sea surface. The surface cooling due to the passage of Hurricane Felix undoubtedly had a significant impact on the seasonal heat budget for the Bermuda region for the summer and fall of 1995. The effect is similar in some ways to that observed by *Large et al.* [1986] for fall storm-generated episodic cooling in the subarctic North Pacific. Temperature profiles collected before and after the passage of Felix are used to estimate heat content changes in the mixed layer and thermocline, i.e. the extent of prolonged cooling.

[9] Felix caused significant changes in the temperature structure of the upper ocean. Surface temperatures decreased by 3.0°–3.5°C to 25°–26°C over a 400 km wide swath centered on the mooring site (Figure 1). The swath was centered 200 km to the right of the hurricane track. Temperature at 25 m decreased to values of 25°C (change of

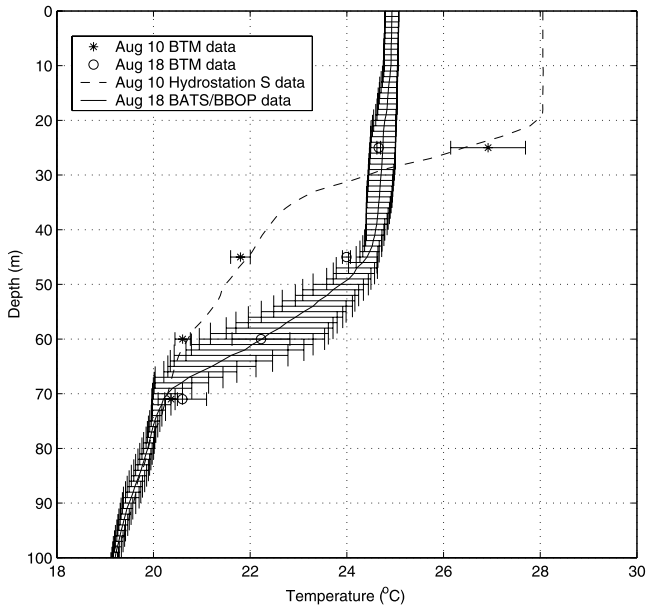

Figure 3. Pre- and post-Felix temperature profiles. Data from Hydrostation S for 10 August and average profile from BBOP/BATS for 18 August are shown along with BTM values averaged over those days. The error bars are ±1 standard deviation from the mean.

~1.5°C) and there was net warming of 1.7°C and 0.9°C at 45 and 60 m, respectively (Figure 2b). There was almost no net change in temperature at 71, 120, and 150 m. Near-inertial oscillations in temperature evident after the passage of Felix indicate the presence of large amplitude internal gravity waves in the thermocline (60 and 71 m).

[10] The mixed layer deepened to 46 ± 4 m (N = 7) according to an average of ship-based temperature profiles taken on 18 August (Figure 3) as part of the BATS and BBOP sampling programs, and to <45 m based on BTM data (Figure 2b). The difference between these estimates likely reflects a combination of spatial variability in the mixed layer depth (the two sampling sites were several kilometers apart) and the coarser vertical resolution of BTM temperature sensors. The BTM's 45 m sensor was near the top of the thermocline after the hurricane (Figure 2).

[11] The depth-integrated heat anomaly (DIH) was calculated [following *Large et al.*, 1986] for vertical intervals where there was net cooling ($[z_1,z_2]$ = [0, 29 m]) and net warming ([29, 70 m]), as well as over the primary domain affected by hurricane mixing ([0, 70 m]); the lower bound is defined as the depth at which there is no significant change in the temperature with time. For details of the calculation, see Appendix A. The temperature records and model results indicate that heat exchange was primarily confined to the upper 70 m (DIH_{0-70} = −51.2 ± 86.6 MJ/m^2). Scale analysis suggests that mixing observed at the BTM site was to first order in the vertical dimension [*Dickey et al.*, 1998a]. The significant heat loss from the upper layer (DIH_{0-29} = −326.4 ± 22.0 MJ/m^2) was partially balanced by that gained in the lower layer where heat exchange occurred (DIH_{29-70} = 275.2 ± 81.4 MJ/m^2). The net heat gained at the surface over the period 10–18 August was ~35 MJ/m^2 (error bars are not reported, but are large). A simple balance based on these estimates suggests that up to ~86 MJ/m^2 of heat (net heat lost out of mixed layer - net heat gained in thermocline; i.e., 26% of the heat lost from the mixed layer) could have been advected horizontally, but we stress that these quantities are also nearly balanced within the large variability of the measurements. The variability in the temperature profiles collected on 18 August reflects vertical displacements of the seasonal thermocline caused by near-inertial internal gravity waves. Intense vertical mixing associated with Felix caused net downward transport of heat below the mixed layer, extending well into the thermocline, between 45 m and 70 m (Figure 4). Note that the adjusted heat profile in Figure 4 (dashed line) was computed by adding 68 MJ/m^2 of heat over the top 70 m of water to account for processes such as horizontal advection and uncertainty in surface heat flux. The adjusted profile is an approximation of how a one-dimensional ocean might have responded to the hurricane, and serves as an additional indicator of model skill (since the models conserve heat in the vertical dimension).

4.2. Currents and Energy Analysis

[12] Hurricane Felix caused a dramatic increase in kinetic energy and complex dynamics in the upper ocean. To characterize the dynamic response to Felix, calculations of the amplitude and kinetic energy of the near-inertial currents using complex demodulation (following *Qi et al.* [1995, equation (A2)]); amplitude of D(τ) shown in Figure 5) were made. During the storm-forced period (13–15 August), large near-inertial currents were observed in the mixed layer. A weaker near-inertial signal was also observed at 106 m, suggesting that near-inertial energy penetrated the thermocline. Curiously, there is not a clear near-inertial oscillation at 71 m, near the base of the strong seasonal

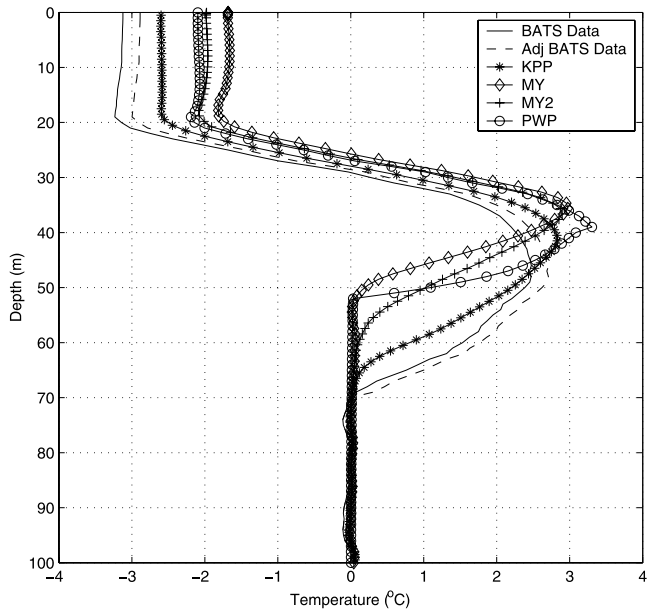

Figure 4. Simulated (from most realistic forcing) and measured (from BBOP/BATS casts) profiles of temperature changes (°C) in the upper 100 m of water. The 10 August temperature profile was subtracted from the average temperature profile for 18 August (N = 7).

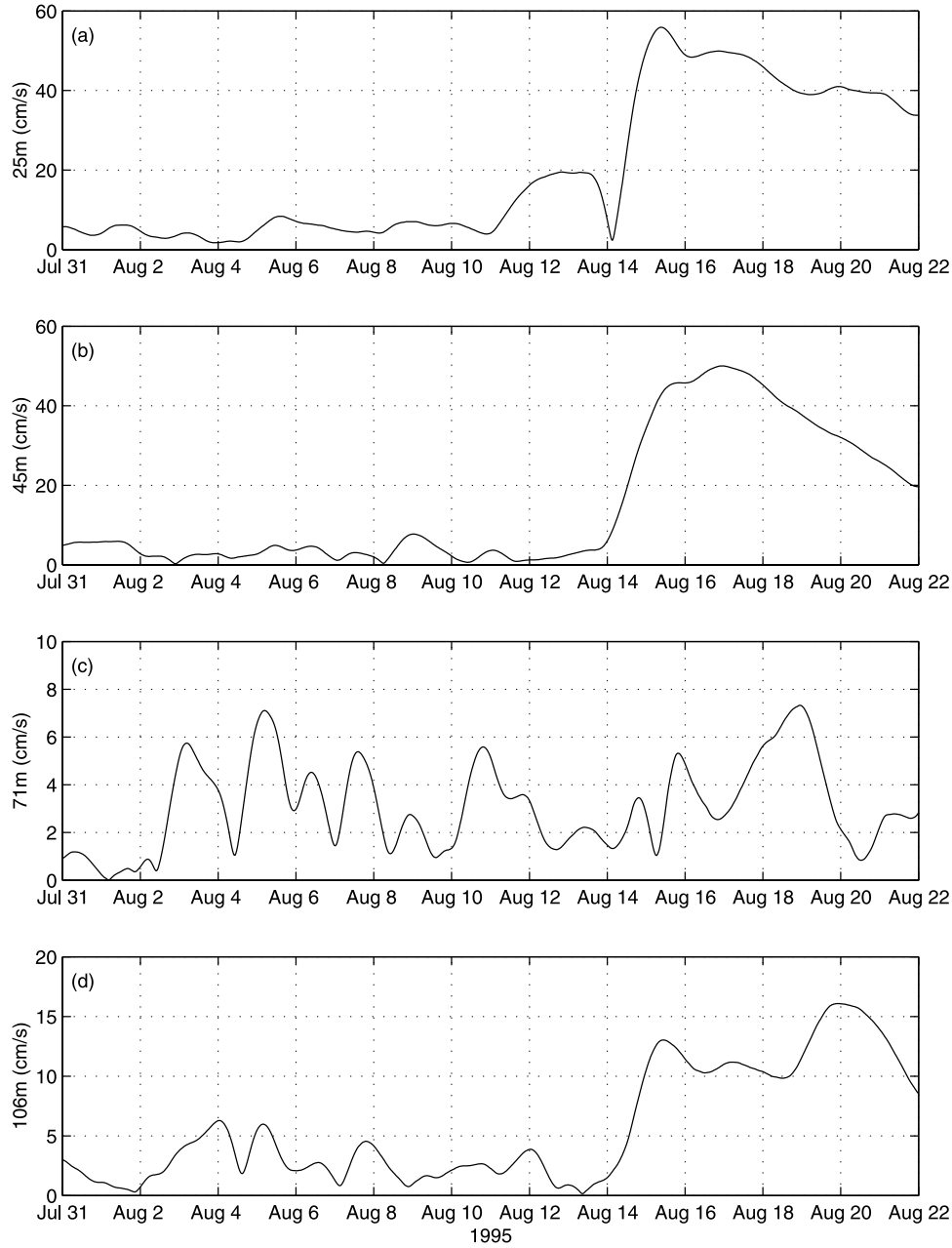

Figure 5. Complex demodulated inertial current amplitude (cm/s) at (a) 25, (b) 45, (c) 71, and (d) 106 m.

thermocline. One possibility is that this signal could have resulted from inertial beating that has been observed previously in response to a storm [*Qi et al.*, 1995]. This effect has been described to occur when the first internal gravity wave mode becomes out of phase with the higher modes, allowing efficient transfer of energy below the thermocline [*Levine and Zervakis*, 1995; *Qi et al.*, 1995; *Zervakis and Levine*, 1995]. At in-between depths, the different modes, which oscillate at different frequencies, interfere and the time series resembles a beat frequency. During the poststorm period, mixed layer currents decayed steadily (winds were comparatively low) and there was a slight increase in currents at 106 m, suggesting downward propagation of energy.

[13] Near-inertial current speed amplitudes reached values of 55 cm/s at 25 m (Figure 5). For comparison, these were about twice those measured during the Ocean Storms experiment [*Qi et al.*, 1995; *Levine and Zervakis*, 1995]; this is expected because of the greater strength of the observed Hurricane Felix winds. There were also significant increases in inertial kinetic energy at 25, 45, and 106 m depth. The poststorm near-inertial amplitude increased by factors of 2.5, 9.0, and 3.3 at these respective depths. The near-inertial kinetic energy was lower at 71 m. The increase in-depth integrated inertial kinetic energy for the mixed layer (ΔIKE_{25}; see Appendix A for calculation details) was 4.6 ± 0.8 kJ/m^2. This value was changed very little when the analogous calculation was made for the upper 45 m of water because prestorm currents at 45 m were small and therefore did not contribute much energy to the integral (Figure 5). This result reflects the deepening of and the large amount of wind energy introduced to the

mixed layer, as well as the prevalence of near-inertial motion there.

[14] Estimates of the *e* folding decay times of the complex demodulated amplitudes (Figure 5) were 14.9 days at 25 m and 5.1 days at 45 m. At 106 m, the inertial component of motion slightly increased until 19–20 August. It should be noted that the reliability of these estimates is limited by the short duration of the poststorm record (~8 days; unfortunately, the mooring had to be recovered because of ship scheduling). It is not surprising that the decay rate was higher at 45 m than at 25 m. Motions at the base of the mixed layer are likely to undergo the most vigorous decay because of the prevalence of a number of processes there. These include: (1) radiation of energy by internal gravity waves [e.g., *Pollard*, 1970; *Price*, 1983; *D'Asaro*, 1995a, 1995b; *D'Asaro et al.*, 1995], (2) turbulence generated through high shear at the base of the mixed layer/thermocline interface caused by extreme, impulsive wind-forcing [*Herbert and Moum*, 1994], and (3) nonlinear transfer of energy from near-inertial waves to high frequency internal waves [*Henyey et al.*, 1986]. Additionally, it is possible that elevated energy levels near the surface were maintained in part by posthurricane winds causing a reduced decay rate at 25 m.

5. Model Initialization and Surface Forcing

[15] The surface heat flux and wind-forcing time series were constructed using mooring measurements [*Dickey et al.*, 1998c, 2001] of wind speed and direction, and visible spectral downwelling irradiance (at seven wavelengths) to estimate incident shortwave radiation. Details explaining the construction of the surface forcing are provided in Appendix B; a brief summary is presented here. Measurements of relative humidity and air temperature were unavailable, so the relative humidity was set to a climatological average of 78% during low winds and 95% during the storm-forced period. The climatological value falls within the range of average measured relative humidity for later sampling periods (covering the period 1996–1999; relative humidity was unavailable in 1995) of the BTM (72–84%). For air temperature, we used NCEP/NCAR reanalysis data [*Doney et al.*, 1998]. Importantly, there was good agreement between these data and data collected during later BTM deployments [*Dickey et al.*, 2001].

5.1. Initial Temperature Profile

[16] Because of the limited number of available thermistors, measurements were too coarsely spaced in the vertical to clearly resolve thermocline structure, and temperature and salinity profile data collected near the BTM were unavailable just prior to the passage of Felix (BATS/BBOP profiles closest in time to the hurricane were collected on 19 July). However, there was good agreement between profile data collected at Hydrostation S and BTM temperatures for 10 August (Figure 3). Thus, these profile data were deemed to be roughly representative of conditions at the BTM site and were used to initialize simulations. To meet the goal of isolating the upper ocean response to hurricane force winds, the simulations were initialized on a date as close as possible to the hurricane passage (on 13 August as opposed to 10 August). By 13 August, BTM temperatures had changed by a maximum of a few tenths of a degree, which is within model forecast errors for a few days. Simulations initialized with measured versus assigned constant salinity produced no perceptible differences in model results. The high vertical resolution profile data are preferable for model initialization because they allow better definition of the mixed layer depth, stratification below the mixed layer, and the storm-induced temperature profile changes in the upper ocean (i.e., redistribution of heat). Mixed layer models are highly sensitive to these parameters. The BTM data were used for temporal comparisons with model results.

[17] Horizontal current components were set uniformly to zero for all models, partly because the current data were available at only four depths. The near-inertial currents observed at 25 m prior to the passage of Hurricane Felix had amplitudes of ~20 cm/s (Figure 2e), and likely interfered with storm generated currents. This issue is addressed in section 8.

5.2. Wind-Forcing

[18] The parameterization of wind stress is a subject of current controversy. On the one hand, there is evidence for a linear relationship between drag coefficient and wind speed [*Garratt*, 1977; *Large and Pond*, 1981; *Yelland and Taylor*, 1996]. On the other hand, there is research supporting the view that drag coefficients can be significantly affected by sea state [*Donelan et al.*, 1993, 1995, 1997; *Donelan*, 1998]. Specifically, using a data set comprised of shipboard measurements from Lake Ontario, the North Sea off the Dutch coast, and an exposed site in the Atlantic Ocean, *Donelan et al.* [1993] and *Donelan* [1998] show that the drag coefficient can be parameterized as a function of wave age (defined as c_p/U_{10}, where c_p is the phase speed of surface waves at the spectral peak, and U_{10} is the wind speed measured at 10 m) in the absence of swell (with younger waves corresponding to higher drag coefficients). Using shipboard data from a site off the coast of Virginia, they show that drag coefficients are elevated in the presence of cross-wind and counterwind swell [*Donelan et al.*, 1997]. For example, the relationship derived by *Donelan et al.* [1993, 1995] suggests that at wind speeds of 25 m/s, the drag coefficient is 50% larger for a wave age of $c_p/U_{10} = 0.2$ than for one of 1.0. Additionally, it is widely acknowledged that more high wind speed data over the open ocean are needed [*Taylor*, 2000]. Notably, wind speeds >20 m/s comprised only ~4% of the *Yelland and Taylor* [1996] data set, which contained shipboard measurements collected over the open Southern Ocean. In addition to the lack of data at high wind speeds, there are problems inherently associated with reconciliation of differences between studies that used data collected in a variety of environments which may be characterized by different dominant physical processes, for example, lakes, open ocean, and coastal sites.

[19] Studies showing sea roughness to be important are contested by *Yelland et al.* [1998], who do a careful analysis of wind distortion by a ship, and show that the scatter about the mean linear drag coefficient/wind speed relationship found by *Yelland and Taylor* [1996] is much reduced when four differently located anemometers were corrected for flow distortion. Also, of particular relevance for this study, they show that changes in the wind stress during a storm

when winds rose to >23 m/s were highly correlated with changes in the direction of the wind stress relative to the ship heading, but not the true wind direction or the wind speed. Their interpretation was that in previous studies, changes in the relative wind direction could have accounted for anomalously high drag coefficient estimates instead of a change in sea state. They conclude that in the open ocean, the drag coefficient is independent of the wave age, while acknowledging that swell, which has been shown to obscure this relationship [*Donelan et al.*, 1993], was likely present during the bulk of their observations. They also note the possibility that special cases may exist. Although we have no wave data to characterize the sea state at the BTM site during the highest winds, we cannot discount the possibility that a hurricane is such a special case, given the implications of previous research.

[20] A separate issue concerning the validity of our wind stress estimates pertains to the fact that measurements of wind speed were from a buoy platform under high winds, instead of from a wind tower or ship. Buoys have the advantage over ships of much reduced flow distortion by the platform, and the disadvantages of the motion of the buoy itself, the fact that buoy mounted wind sensors sit low in the water (i.e., below 10 m), and possible effects of wave sheltering, which could bias measurements toward lower values [e.g., *Dickey et al.*, 1998a]. We note that many formulations of the drag coefficient [*Garratt*, 1977; *Large and Pond*, 1981; *Yelland and Taylor*, 1996; *Yelland et al.*, 1998] are based on shipboard measurements, so we cannot discount the possibility that different parameterizations might be established if buoy winds were used instead. Toward this end, *Large et al.* [1995] found a wave sheltering effect in their comparison of NCEP/NCAR assimilated winds and in situ observations from moored and drifting buoys, and forward a wind speed correction for wave distortion. It remains unknown whether this correction is necessarily appropriate for wind-forcing for hurricanes. Surface waves should reach extreme heights, but may not be in equilibrium with the wind field for a tightly spun cyclone. Additionally, any empirical adjustment is difficult to formulate both because of the paucity of buoy data and the lack of an accepted standard for hurricane winds to compare against the available data. During most of the deployment, wind stress correlated moderately well (r^2 = 0.60; r^2 = 0.57) with the NCEP/NCAR reanalysis data used for surface momentum flux calculations by *Doney et al.* [1998], but there was no apparent relationship between these data products during the hurricane (when buoy measurement-based estimates of wind stress were 175% higher). This is not surprising considering that NCEP/NCAR wind data are based on a model assimilation product with spatial resolution too coarse (1.5° or ~150 km) to properly resolve hurricane winds. Hurricane diameters are typically O(~300 km) and radial gradients are strong. However, we cannot preclude the possibility that some wave sheltering may have occurred, even if the correction is different from that presented by *Large et al.* [1995].

[21] A third issue involves the determination of wind stress vectors from measured wind speed and direction with respect to models. A key difficulty in this calculation is in the estimation of the wind work; *Price* [1983] parameterizes this as the cumulative integral of wind stress vector dotted into the surface current vector; in other words, the magnitude of wind work depends on the angle between the wind direction and the surface current direction. Two problems in making a calculation of the wind work using BTM measurements are: (1) we do not have complete confidence in the accuracy of our wind speed direction and (2) the shallowest measurements of current speed are at 25 m; by this depth, the currents would have significantly changed in magnitude and direction from those directly at the surface. *Price* [1983] avoids this problem because he uses a slab model (where the currents are uniform in both speed and direction over the top 50 m of water). Both of these problems undermine the validity of the wind work calculation. For the models, the wind work was nearly balanced by the sum of depth integrated kinetic and potential energy (to 100 m depth). However, the wind work estimated from the data is much higher than the sum of depth integrated kinetic and potential energy. This suggests that there are likely problems with the relative direction of the wind and surface currents (as mentioned above) and/or that there is significant energy loss across the sea surface based on data, but not in the models.

[22] For the main simulations in this paper (case I), we have chosen the linear drag coefficient parameterization of *Garratt* [1977], which results in wind stress that is on average 15.1% higher than that using *Large and Pond* [1981], and 3.5% higher than the *Yelland and Taylor* [1996] parameterizations for the interval 15–35 m/s, within the range of highest winds observed during Hurricane Felix. This is in keeping with studies supporting a linear relationship between drag coefficient and wind speed [*Garratt*, 1977; *Large and Pond*, 1981; *Yelland and Taylor*, 1996; *Taylor*, 2000]. Credence is also given to the possibility of adjustments to the calculation of wind speed or wind stress that may be appropriate to account for the possible effects of wave sheltering on the measurements [*Large et al.*, 1995] or of the presence of young waves during the highest winds [*Donelan et al.*, 1993, 1995]. These effects are treated in sensitivity simulations. Although we can use our results to suggest whether such corrections are necessary, it is not within the scope of this paper to challenge current thought on the drag coefficient parameterization [*Taylor*, 2000], but rather to suggest that for high wind stress during storms, more research needs to be done to resolve the issues. The issue of wind stress calculations is highly controversial, and likely arises in part from differences in studies using different platforms in a variety of diverse environments, particularly under the influence of varying sea states.

[23] The cases considered are as follows: (1) case I: BTM 4.2 m winds adjusted to 10 m with drag coefficient correction for atmospheric stability following *Garratt* [1977] and (2) case II: BTM 4.2 m winds adjusted to 10 m with drag coefficient correction for both atmospheric stability following *Large and Pond* [1981] and wave distortion [*Large et al.*, 1995]. The case II wind stress values were much higher than those computed without wave distortion. A third case, resulting in intermediate wind stresses between the case I and case II wind stress values, was constructed by multiplying the case I drag coefficient by a factor of 1.5, to account for the possibility of a young wave field during the highest winds [*Donelan et al.*, 1993,

1995]. This was done for sensitivity purposes, and was therefore only used for a MY2 model simulation. Changes in the surface heat fluxes did not significantly affect the temperature and current evolution predicted by the models; this study was primarily an exercise in wind mixing.

6. Models

[24] Multiple model formulations were used to address three objectives: (1) to estimate the contributions of one-dimensional processes in the upper ocean response, (2) to assess model skill in predicting the response to Hurricane Felix, acknowledging that the fidelity of such a comparison is constrained by the quality of the forcing conditions (wind stress parameterization is a current research topic), and (3) to evaluate differences in model behaviors as they reflect the processes that they are specifically designed to simulate, here with reference to the special application of hurricane forcing. In this way, we address differences among models and the modeled responses. Although the models differ in their formulations, they all mix in response to turbulence produced by velocity shear on various vertical scales and to destabilizing buoyancy fluxes. For all models, solar insolation was parameterized using a double exponential formulation [e.g., *Dickey and Simpson*, 1983a]. Time and depth resolutions were set at 15 min and 1 m for all model simulations for consistency. In the PWP and KPP models, z is positive downward and in the MY and MY2 models, z is positive upwards. For plotting purposes, the coordinate systems are reported with z positive downward. No changes were made in internal parameters.

[25] For the PWP model, turbulent mixing is accounted for implicitly by requiring static, mixed layer, and shear flow stability for the water column [*Price et al.*, 1986]. Static stability is achieved by mixing over grid scale density inversions, or by requiring that

$$\frac{\partial \rho}{\partial z} \geq 0 \tag{1}$$

for the entire water column, where ρ is the depth dependent density of seawater. The base of the mixed layer is deepened until a bulk Richardson number is greater than a prescribed value,

$$R_{bPWP} = \frac{g \Delta \rho h}{\rho_o \left(\Delta S_p\right)^2} \geq 0.65 \tag{2}$$

In equation (2), g is the acceleration due to gravity, h is the depth of the mixed layer, ρ_o is the mean density of seawater, S_p is the horizontal current amplitude, and Δ denotes the difference between the value of the indicated quantity in the mixed layer and at a grid point just below the mixed layer. Once these conditions are satisfied, the stratified region below the mixed layer is smoothed by mixing across grid scale instabilities until the gradient Richardson number is above a prescribed value,

$$R_{gPWP} = \frac{g \frac{\partial \rho}{\partial z}}{\rho_o \left(\frac{\partial S_p}{\partial z}\right)^2} \geq 0.25 \tag{3}$$

where the derivatives are taken for each grid point in the region just below the base of the mixed layer. Turbulent heat fluxes are introduced at the surface grid point; mixing during convective conditions is accounted for by the requirement of static stability.

[26] The MY level 2.5 [*Mellor and Yamada*, 1982] model is a second moment turbulence closure model with prognostic equations for turbulent kinetic energy and a master length scale. Closure is achieved by applying the Kolmogorov hypothesis of local, small scale isotropy to parameterize the viscous terms and the Rotta energy redistribution hypothesis to parameterize the turbulent pressure/velocity moments, both in terms of known variables. The turbulent moments are then written as a function of an isotropic and an anisotropic part and the prognostic equations for these moments are simplified by ignoring all terms with squared anisotropic components. The kinematic moments are parameterized as proportional to mean vertical shear and an eddy viscosity. The eddy viscosity is parameterized as a function of a master length scale, the square root of twice the turbulent kinetic energy per unit mass, and similarity terms that are functions of a local Richardson number

$$R_{gMY} = -\frac{g\beta \frac{\partial T}{\partial z}}{\left(\frac{\partial U}{\partial z}\right)^2 + \left(\frac{\partial V}{\partial z}\right)^2} \tag{4}$$

where β is the thermal expansion of seawater, T is the temperature, and the partial derivatives are defined for each grid point. The internal empirical constants are derived from laboratory results (see *Mellor and Yamada* [1982] for detailed formulations).

[27] A recently modified version of the MY model, the MY2 model, accounts for a reduction in dissipation rate that occurs for locally stable Richardson numbers [*Mellor*, 2001]. The MY2 model utilizes experimental data resulting from a laboratory experiment in which a grid was towed vertically through a stratified fluid initially at rest [*Dickey and Mellor*, 1980]. The mesh Reynolds number (based on grid spacing, grid velocity, and kinematic viscosity of water) was over 48,000. The salient result of the experiment was that turbulent kinetic energy initially decayed inversely with time (very similar to the decay rate for a homogeneous fluid), but then abruptly transitioned to a regime with nearly constant turbulent kinetic energy and a very small dissipation rate. The interpretation is that the field of turbulence was replaced by internal gravity waves when a critical Richardson number (Richardson number R_{gMY2} is defined below) was reached. A model of this effect was developed by *Dickey and Mellor* [1980] and serves as the basis for the Richardson number-dependent dissipation submodel used in MY2. The model equations for the dissipation rate parameterization follow:

$$\begin{aligned}
&\varepsilon = \frac{q^3}{Bl} \Im(G_H), \\
&R_{gMY2} = -B^2 \frac{l^2}{q^2} \frac{g}{\rho_o} \frac{\partial \rho}{\partial z}, \\
&G_H = -R_{gMY2}/B^2, \\
&\Im(G_H) = \begin{cases} 1.0, G_H \geq 0 \\ 1.0 - 0.9(G_H/G_{Hc})^{3/2}, G_{Hc} < G_H < 0 \\ 0.1, G_H \leq G_{Hc} \end{cases}
\end{aligned} \tag{5}$$

where ε is the dissipation rate of turbulent kinetic energy, q^2 is twice the turbulent kinetic energy per unit mass (hereafter q^2 is referred to as turbulent kinetic energy), l is the master

turbulent length scale, G_H is proportional to Richardson number R_{gMY2}, and G_{Hc} and B are empirical constants. This modification allows for increased turbulent kinetic energy in the thermocline under conditions of density stratification. This increase in turbulent kinetic energy effectively leads to enhanced deepening of the mixed layer and lowering of upper layer temperature as compared with the MY model. *Mellor* [2001] has used the MY2 model for simulations of the seasonal cycles at Ocean Weather Stations Papa and November and other sites and found considerable improvement in model comparisons with observations of both temperature and mixed layer depth. A second modification proposed by *Pollard and Millard* [1970] and implemented by *Mellor* [2001] is the application of a constant decay rate for inertial currents. This aspect is discussed at the end of section 7.

[28] In the KPP model [*Large et al.*, 1994], the ocean is decomposed into a planetary boundary layer and an interior (below the depth of the planetary boundary layer), which are characterized by fundamentally different mixing processes. Once diffusivity and viscosity profiles have been calculated for each of these two regions, a smooth profile is generated by requiring these and their first derivatives to match at the depth of the planetary boundary layer. In the planetary boundary layer, mixing is parameterized by an eddy viscosity profile and (under convective conditions and only for temperature) a countergradient term. The strength of the eddy viscosity is driven nonlocally in the boundary layer by surface wind and buoyancy forcing. The eddy viscosity is also proportional to a shape function, which is a smooth profile forcing values of zero at the surface and planetary boundary layer depth. The planetary boundary layer depth, d, is determined as the shallowest depth at which a bulk Richardson number, R_{bKPP}, is greater than or equal to a critical value R_{ic}, i.e., shallowest depth z such that

$$R_{bKPP}(z) = \frac{\left(B_{fr} - B_f(z)\right)z}{|V_r - V(z)|^2 + V_t^2(z)} \geq R_{ic} \tag{6}$$

and is allowed to penetrate below the traditionally defined mixed layer, leading to enhanced entrainment. In equation (6), B_f is the buoyancy, V is the current speed, the subscript r denotes the mean value of the quantity in the Monin-Obukhov surface layer, and $V_t(z)$ is the velocity scale of the turbulent velocity shear. In the interior, the eddy viscosity is strictly local and is set by a gradient Richardson number instability criterion and a (constant) background internal wave term. The Richardson number instability mixing is specified by:

$$\begin{aligned} R_{gKPP} &= \frac{g\left(\frac{\partial \rho}{\partial z}\right)}{\rho_o\left[\left(\frac{\partial U}{\partial z}\right)^2 + \left(\frac{\partial V}{\partial z}\right)^2\right]} \\ \upsilon &= \upsilon_o, R_{gKPP} < 0 \\ \upsilon &= \upsilon_o\left[1 - \left(\frac{R_{gKPP}}{Ri_o}\right)^2\right]^3, 0 < R_{gKPP} < R_{gc} \\ \upsilon &= 0, R_{gc} < R_{gKPP} \end{aligned} \tag{7}$$

where R_{gKPP} is the gradient Richardson number with partial derivatives defined at single grid points, U and V are east and north mean horizontal current components, υ is the eddy viscosity, and υ_o and Ri_o are constants. These conditions allow enhanced mixing and (because of the viscosity profile matching conditions at the boundary layer depth) can result in a deeper boundary layer.

7. Model Results

[29] The wind-forcing for all simulations follows the case I formulation as described earlier (Figure 6). Modeled sea surface cooling was between 1.7 and 2.6°C and mixed layer depth values ranged between 36.5 and 44.2 m (Figure 7; Table 1). Additionally, the change in depth–integrated potential energy for the top 100 m (time series calculation adopted from *Price* [1983, equation (12)]) was comparable to that estimated for the observations. Although the simulated ranges of sea surface cooling are generally less than those observed, modeled values are affected to some extent by the parameterization of the heat loss at the surface (Appendix B). Sensitivity analyses indicate that uncertainty in the latent heat flux alone could account for 0.1–0.2°C of additional cooling and that overall, surface heat loss accounted for 0.3–0.5°C (or 15%) of the simulated cooling response; this is consistent with findings for Hurricane Elouise [*Price*, 1981; *Martin*, 1982].

[30] The MY, MY2, and PWP models predicted about half to two thirds of the observed heat loss from the surface layer (DIH_{0-29}; Table 2), or ≥1°C less cooling in the mixed layer (Table 1; Figures 4 and 8) than observed. For these models, mixing was minimal or nonexistent between 55 m and 70 m depth (Figure 4) and as a result, temperatures in that depth interval were below those observed (Figure 8). The KPP model predicted a greater extent of vertical mixing (Figure 4), a cooler sea surface temperature (Table 1), and a greater amount of heat lost from the top 29 m of water (DIH_{0-29m}; Table 2) than the other models. This is likely due to the parameterization of gradient Richardson number mixing (R_{gKPP}) in the thermocline and the boundary layer depth scheme, as discussed later.

[31] Modeled and observed north and east current components at 25, 45, 71, and 106 m are shown in Figures 9a and 9b. At 25 m and 45 m, the KPP, MY2, and PWP models predicted horizontal current components within the uncertainties of those observed during the storm-forced and poststorm periods (Figures 9a–9c and 10; Table 3). Depth integrated kinetic energy (over the top 100 m; time series calculation adopted from *Price* [1983, equation (12)]) was comparable to that observed. This is not unexpected, as near-inertial horizontal currents should be primarily locally generated. For the MY simulation, poststorm currents were overestimated at 25 m and underestimated at 45 m, indicating an overestimate of kinetic energy near the surface (the mixed layer was shallower and thus kinetic energy was concentrated over a shallower layer). Note that the specification of the storm-forced period accounts for some bias in the average values of current speeds. The KPP predicted somewhat deeper penetration of near-inertial kinetic energy (~70 m) than the PWP, MY, and MY2 (~50 m; see Figure 9). At 71 and 106 m, there was apparent lack of agreement between observations and all models. A possible explanation for the 71 m current record is inertial beating as described earlier [*Levine and Zervakis*, 1995; *Qi et al.*, 1995; *Zervakis and Levine*, 1995].

[32] For measures of both temperature and currents, disagreements between the simulated and observed proper-

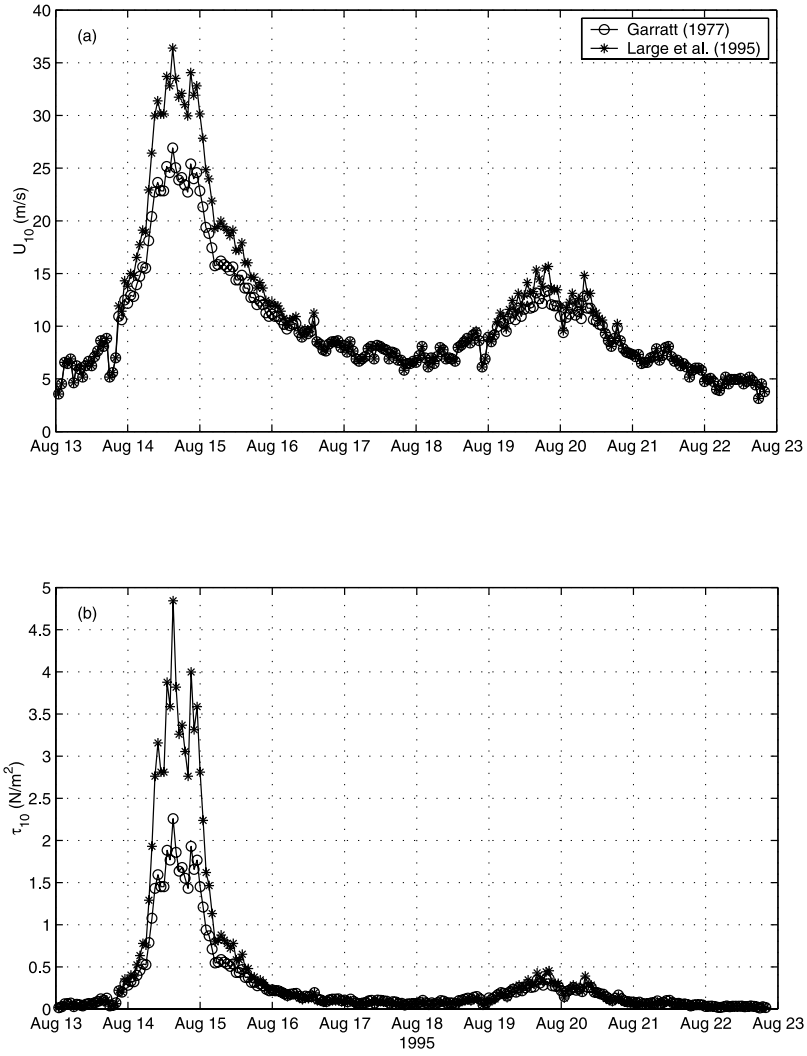

Figure 6. Time series of 10 m wind (U_{10}) and wind stress (τ_{10}) showing wind conditions used to force the models for case I and case II (see Appendix B for details). The open circles represent the 10 m winds and wind stress with no correction for wave distortion as specified by case I forcing and the asterisks represent the 10 m wind and wind stress corrected for wave distortion as given by *Large et al.* [1995] as specified by case II forcing. (a) Wind speed at 10 m (m/s) and (b) wind stress at 10 m (N/m^2).

ties can probably be attributed in part to three-dimensional lateral affects including propagation and interaction of internal waves and inertial pumping, which probably acted to invigorate mixing in the thermocline and propagate kinetic energy at depth. At the same time, the success of the models in predicting reasonable estimates of mixed layer near-inertial currents suggests that the upper layer response was primarily forced locally.

[33] As discussed earlier, the appropriate calculation method for wind stress for high wind conditions is uncertain. Toward this end, we applied case II forcing to the models. Under case II forcing, cooling of the sea surface exceeded that observed by $\sim$1°C, and mixed layer depth was overestimated by 12–19 m for the KPP and PWP models. Analogously, depth integrated (to 100 m) kinetic plus potential energy was much higher than observed. The MY2 (Figure 9c) and MY temperature predictions were much improved, with more reasonable estimates of mixed layer depth. In the case of the MY simulation, mixed layer currents were considerably higher than for the other models; this behavior is consistent throughout this study and with the findings of previous mixed layer model intercomparison studies [e.g., *Martin*, 1985; *Large and Crawford*, 1995]. However, for all of the models, kinetic energy input to the mixed layer was overestimated by a factor of 3–6, and for this reason, we conclude that application of the *Large et al.* [1995] correction for wave distortion is not appropriate, at least in its present form, for the case of Hurricane Felix. This does not preclude the possibility that a smaller increase in wind stress may be appropriate, whether due to a wave sheltering effect or the presence of young waves during high winds. To address this issue, we forced the MY2 model, which produced the smallest increases in inertial kinetic energy to the mixed layer for a proportionate increase in wind stress, with a drag coefficient increased by a factor of 1.5, following *Donelan et al.* [1995]. This produced a remarkable improvement in agreement with the temperature evolution, but not without increasing the currents to higher

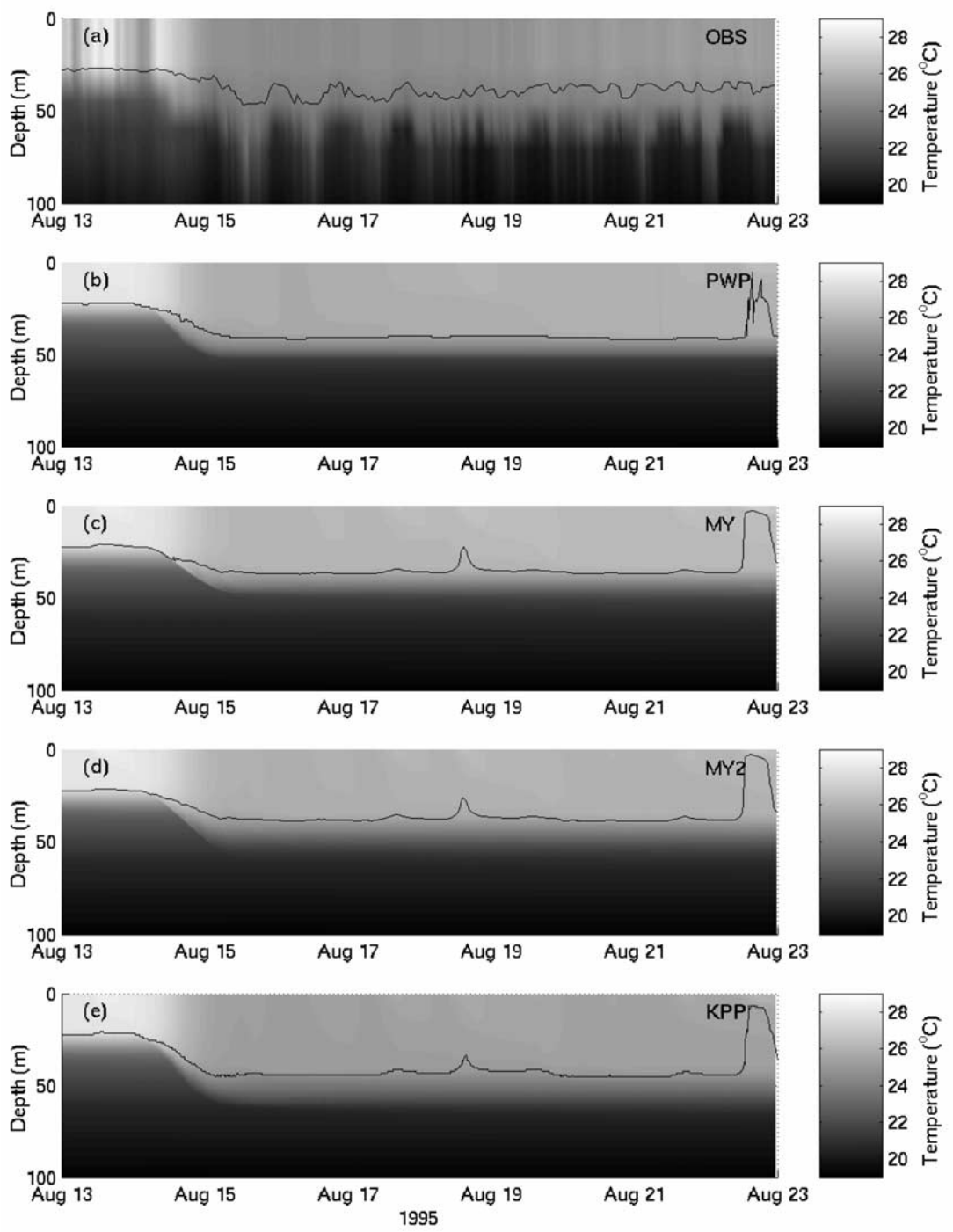

Figure 7. Simulated temperature evolution over the upper 100 m of water for the observations and models. Simulated mixed layer depth time series (based on a 0.5°C criterion) are overlaid. All model results are for case I forcing. These quantities are shown for (a) observations, (b) PWP, (c) MY, (d) MY2, and (e) KPP model simulations.

levels (Figure 9c). Specifically, the inertial current energy input to the mixed layer increased from 5.6 kJ/m^2 for case I forcing to 9.3 kJ/m^2 (as compared to 4.6 kJ/m^2 observed), with currents at 45 m increasing from ~40 cm/s to 80 cm/s. Based on the case II results, we expect the increase to be larger for the other models. For case I forcing, the KPP simulation came closer to predicting both horizontal currents and temperature evolution than any of the other models, and for the *Donelan et al.* [1993] forcing, the MY2 model very nearly reproduced the observed temperature evolution, although currents are clearly overestimated.

[34] Sensitivity experiments support results from previous studies [*Pollard and Millard*, 1970; *Mellor*, 2001] that show use of a scheme for constant inertial decay can improve

Table 1. Cooling at the Sea Surface, ΔT, and Post-Felix Mixed Layer Depth, MLD_f, According to the BATS/BBOP Profiles and the BTM Data for Case I and Case II Wind Stress Forcing[a]

	ΔT, °C		MLD_f, m	
	Case I	Case II	Case I	Case II
OBS	3 to 4	3 to 4	46 ± 4[b], <45[c]	46 ± 4[b], <45[c]
MY	1.7	2.8	36.5	44.0
MY2	2.0	3.0	38.0	44.0
PWP	2.1	4.2	40.6	57.8
KPP	2.6	4.3	44.2	67.3

[a]In this table, ΔT(°C) represents SST cooling, and MLD_f is the post-Felix mixed layer depth. Both case I and case II wind stress time series are based on the observations; case II differs from case I primarily in that it includes a correction for wave distortion constructed by *Large et al.* [1995]. Notably, case II wind stress magnitudes during the storm passage were close to twice those of case I (Figure 6) and resulted in much deeper mixed layers and more cooling at the sea surface than observed for the PWP and KPP models. The mixed layer currents for case II forcing were much higher than observed. See Appendix B for construction details of case I and case II wind stress time series.

[b]MLD calculated using the 0.5°C criterion BATS/BBOP profiles collected on 18 August.

[c]MLD indicated by BTM data on 18 August.

simulations of poststorm currents and kinetic energy in one-dimensional models. When the MY2 model was modified to include constant decay timescales of $\tau_D = \infty$ (base model case with no decay), $\tau_D = 8$ inertial days (as suggested by *Mellor* [2001]), and $\tau_D = 15.7$ inertial days (the latter value based on BTM data), the undamped simulated currents were ~50–100% higher than their damped counterparts by 23 August (Figure 9d).

8. Sensitivity Experiments

[35] Sensitivity experiments were conducted to assess the effect of preexisting near-inertial currents on poststorm motion, and possible resonance/antiresonance effects that may have occurred due to clockwise (CW) or counterclockwise (CCW) rotation of the wind stress during passage of the hurricane. The experiments were performed with the KPP and MY2 models and were forced with one or two wind pulses, each of two days duration.

[36] For all experiments, the observed Hurricane Felix wind stress magnitude (i.e., case I forcing) was used to represent the storm pulse. A small ambient wind stress (τ = 0.014 N/m^2) was applied to prevent unphysical heating of the mixed layer. A constant, positive, heat flux equal to the mean heat flux for the integration period 13–23 August (as opposed to a diurnally varying heat flux; ~46 W/m^2) was applied to prevent periodic shoaling of the mixed layer that can significantly affect simulated dynamics (which we were attempting to isolate) and structure near the surface, and that has been shown to occur when there is a phase lag between winds and heating [*Dickey and Simpson*, 1983b]. These adjustments did not appear to appreciably affect currents at 25 m.

[37] The effect of preexisting inertial currents was investigated by applying a small wind pulse approximately two days prior to the hurricane. A set of three simulations was conducted varying the exact interval between the initial wind pulse and hurricane by 12 hours or approximately half an inertial period. The time intervals between the two pulses are denoted in hours (as t') as the time between the trailing edge of the first pulse to the leading edge of the following pulse. The wind stress time series of the first event was a scaled down version of the hurricane wind stress. The magnitudes were separately adjusted for each model to produce current speeds of around 20 cm/s at 25 m, which fall exactly in the middle of the range observed at that depth. This was about 22% and 27% of the maximum wind amplitude observed for Felix for the KPP and MY2 models, respectively. Similar results were obtained for both models, so only the KPP results are shown in the figures.

[38] Three sensitivity experiments were performed.

1. Case III: For this experiment, the models were forced with two pulses. Wind stress direction during the storm was as observed (i.e., from case I forcing).
2. Case IV: The models were forced by one wind pulse with an imposed near-inertial rotation of the wind stress vectors in both CW and CCW directions with ~11 h duration. Note that CW (CCW) is the expected sense of wind stress rotation that would have been observed by a mooring on the right (left) side of the storm track. The storm winds were initially directed to the southwest, which is the direction that they would have been moving for the theoretical case of a symmetric hurricane in gradient balance approaching from the southeast of the mooring (wind direction along tangents to circles concentric about the eye; i.e., no inflow angle), and were rotated to the northeast through half an inertial period. An additional sensitivity test was performed with zero rotation (constant direction of winds to the southwest).
3. Case V: The models were forced with two wind pulses (separated by the same time intervals and with the same wind stress magnitude used for case III), and the CW and CCW rotation imposed for the second storm from case IV.

8.1. Case III: Effect of Preexisting Near-Inertial Current Oscillations on Poststorm Response

[39] Sensitivity experiments support the hypothesis that the phase of preexisting near-inertial currents present before the passage of Hurricane Felix significantly affected the amplitude of poststorm near-inertial currents [*Crawford and Large*, 1996]. Mean poststorm current speed at 25 m varied in a sinusoidal fashion with respect to pulse separation (trailing edge of pulse to leading edge of following pulse), with extrema at 8 h (weakest response) and 20 h (largest response). Note that because the pulses were not instantaneous pulses or square waves, the poststorm current extrema were not found at the theoretical solution separation times of half the inertial period and the inertial period (11.4 h and 22.8 h for Bermuda), but rather at 8 h and 20 h. The results of this sensitivity experiment suggest that during the storm-

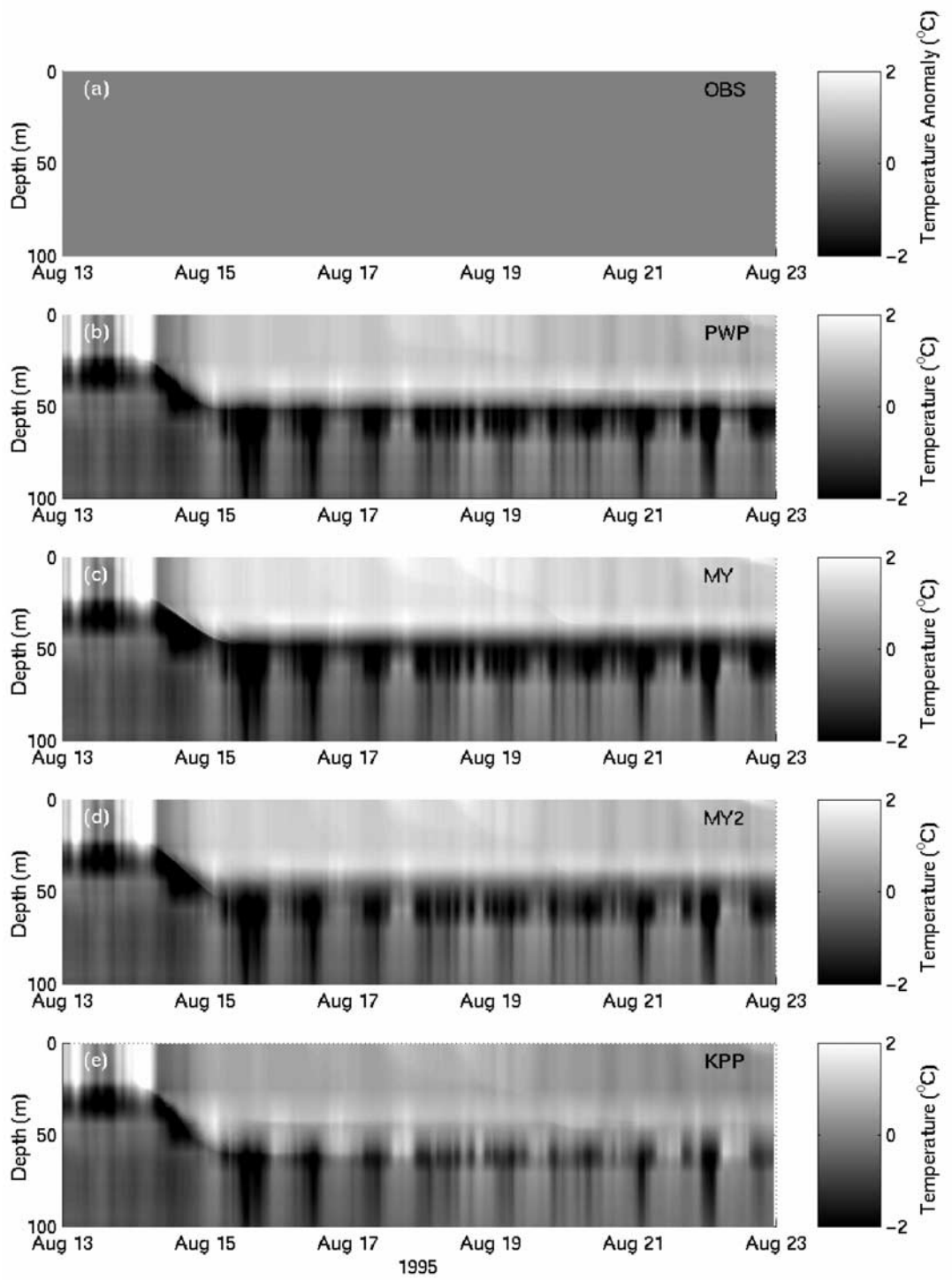

Figure 8. Difference between simulated and observed temperature evolution over the upper 100 m of water. All model results are for case I forcing. (a) Observations – observations, (b) PWP – observations, (c) MY – observations, (d) MY2 – observations, and (e) KPP – observations.

forced and poststorm periods, the 25 m currents would be ~50% higher for a pulse separation of 20 h versus one of 8 h. Specifically, the poststorm 25 m current speeds ranged between 41 and 69 cm/s (50 cm/s and 76 cm/s for the MY2 model) when the pulse separation time was varied between 8 h and 20 h (which resulted in minimum and maximum current speeds). Our interpretation of this behavior is that for $t' = 20$ h, the prestorm generated currents were in phase with the storm-generated currents (constructive interference) while the poststorm currents were out of phase with the storm generated currents (destructive interference). MLD and ΔSST did not change very much when the time between the wind pulses was varied over an inertial period, suggesting that water column stratification was high and

Table 2. Depth Integrated Heat Anomaly Calculated Using Equation (A1) for the Models and Observations and for the Following Depth Intervals: 0–29 m (DIH_{0-29}), 29–70 m (DIH_{29-70}), and 0–70 m (DIH_{0-70})[a]

	DIH_{0-29}, MJ/m^2	DIH_{29-70}, MJ/m^2	DIH_{0-70}, MJ/m^2
OBS	−326.4 ± 22.0	275.2 ± 81.4	−51.2 ± 86.6
MY	−155.3	164.1	14.5
MY2	−189.1	199.6	15.1
PWP	−200.5	217.3	16.8
KPP	−253.8	269.0	17.0

[a]Notably, the observed value of DIH_{0-70} is negative. Considering that there was net warming of the ocean during the integration period, this may reflect horizontal advection of heat away from the mooring site as well as errors due to variability in the measured temperature profile.

mixed layer deepening therefore relatively insensitive to the associated changes in shear (Figure 11).

8.2. Case IV: Effect of Near-Inertial CW/CCW Rotation of Winds

[40] Sensitivity tests with imposed clockwise (CW) and counterclockwise (CCW) rotation at the inertial frequency during the highest winds were performed to find theoretical upper and lower bounds for current speeds produced by Felix (the BTM was likely near the band of maximum winds) and to assess differences in current and temperature evolution that could result from uncertainties in the direction recorded at the mooring site. The most efficient transfer

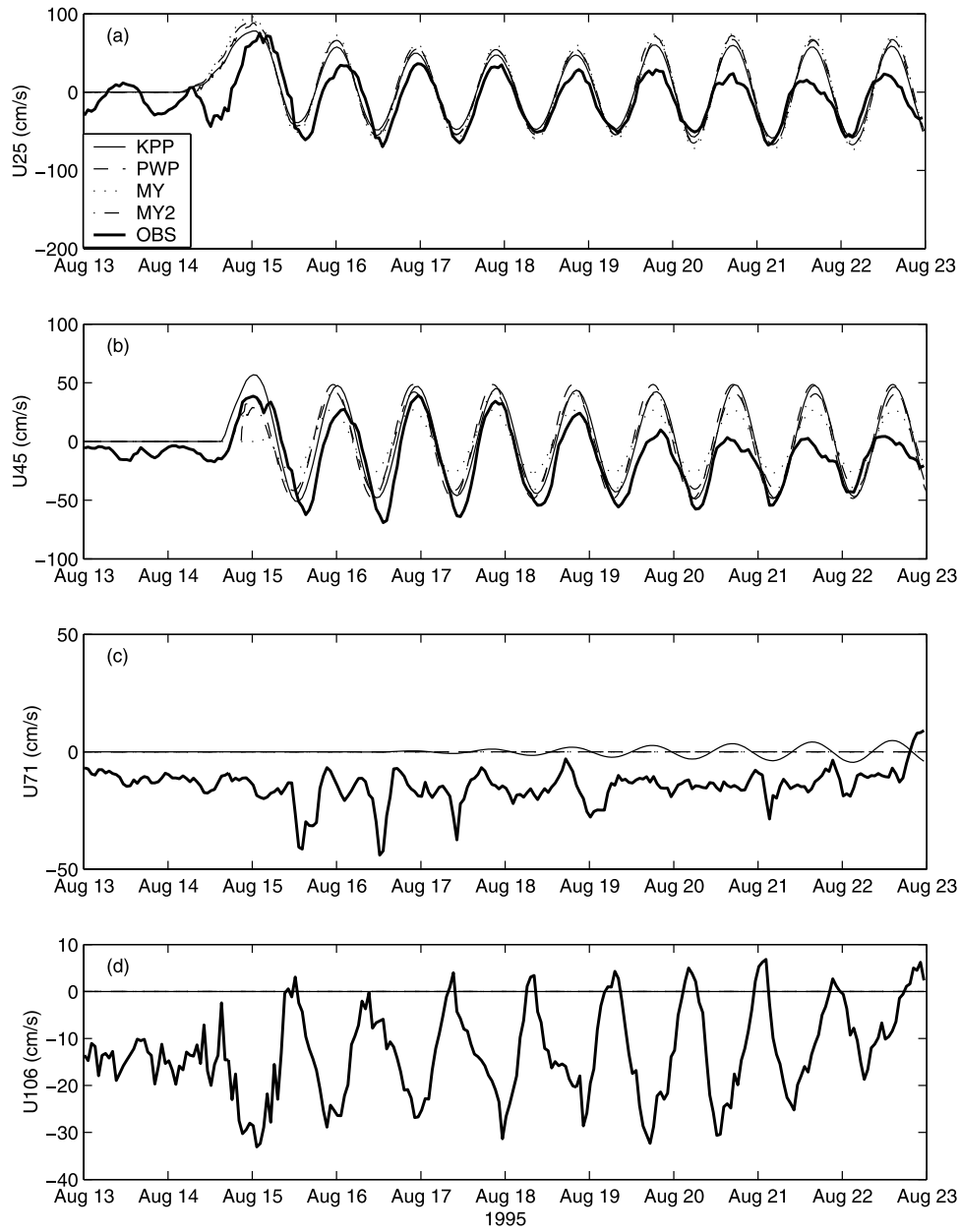

Figure 9a. Simulated east horizontal current U (cm/s) for KPP, PWP, MY, and MY2 models for case I forcing at (a) 25, (b) 45, (c) 71, and (d) 106 m. Observed current record is shown with a solid line. Note that velocity scales are different for the respective depths.

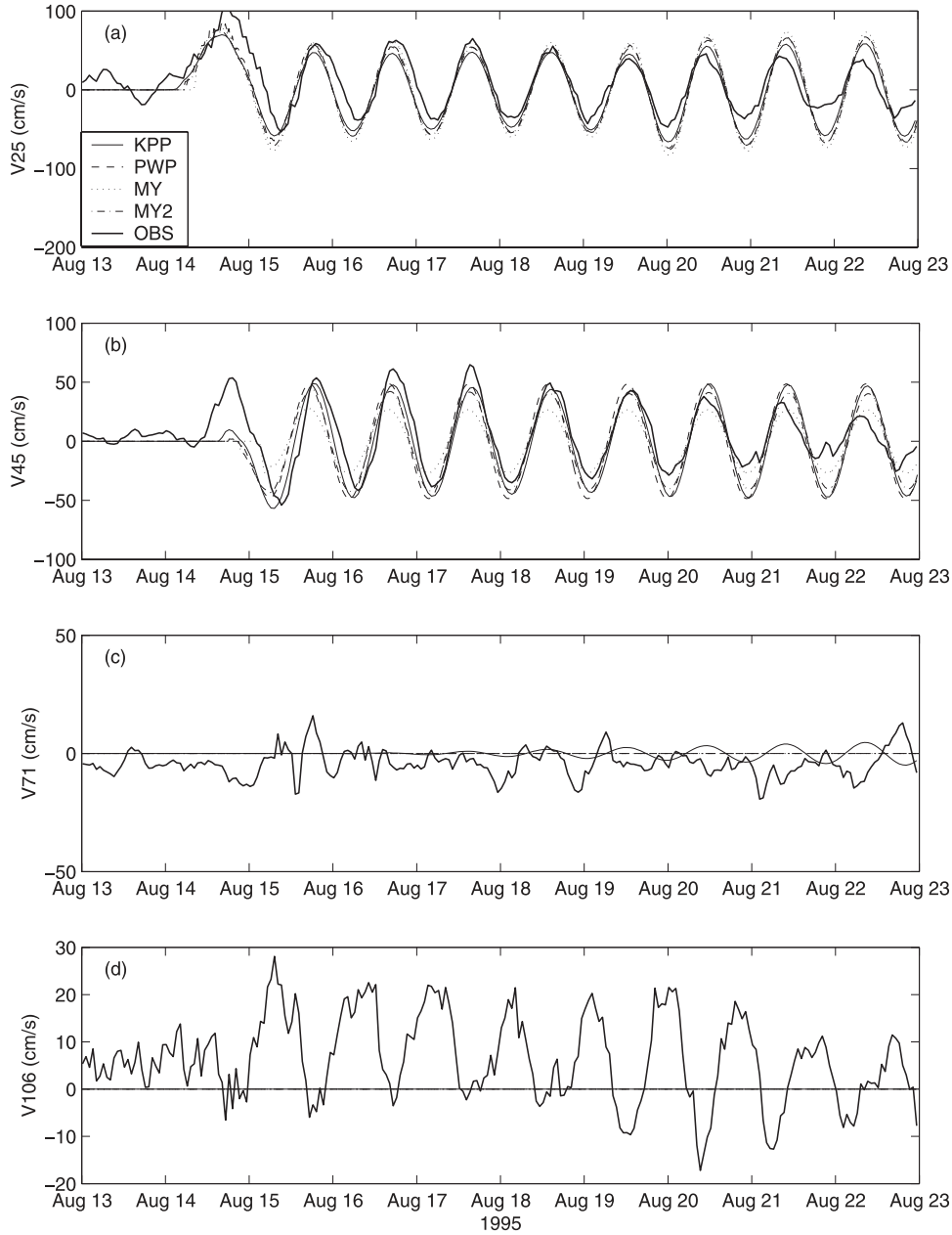

Figure 9b. Same as Figure 9a, but for north horizontal current component (V).

of wind kinetic energy to the near-inertial currents is achieved when the wind rotation is resonant at a near-inertial frequency [e.g., *Dickey and Simpson*, 1983b; *Crawford and Large*, 1996]. Stronger mixed layer currents result in greater shear at the base of the mixed layer, and enhanced turbulent mixing (and hence deeper mixed layers and cooler sea surface temperatures). For hurricanes, this effect is in large part responsible for asymmetrical current strength and cooling underneath the hurricane track (responses are typically much stronger on the right hand side of the storm; see Figure 1 [*Price*, 1981; *Martin*, 1982]).

[41] The sensitivity tests indicated that beneath the maximum band of winds, sea surface temperature decreased between 1.8°–3.8°C (1°–3°C for the MY2 model), mixed layer depths ranged from 40–50 m (30–40 m for the MY2 model), and poststorm near-inertial current amplitudes were between 32 and 122 cm/s (36 cm/s and 141 cm/s for the MY2 model) depending on whether the forcing was CW (largest response) or CCW (smallest response; Figure 12). The fact that our measured and modeled currents have magnitudes that fall well within the current range supports the fidelity of our wind direction measurements, which did not show strong CW rotation (which would be the theoretical expectation on the right side of a hurricane).

8.3. Case V: Combined Effect of Pulsing and CW/CCW Inertial Rotation of Winds

[42] We assessed the combined effect that initial near-inertial currents and resonant wind-forcing during the storm could have on the poststorm dynamics. The results indicate that when there is a strong resonance effect due to CW rotation of the winds, initial inertial currents do not affect

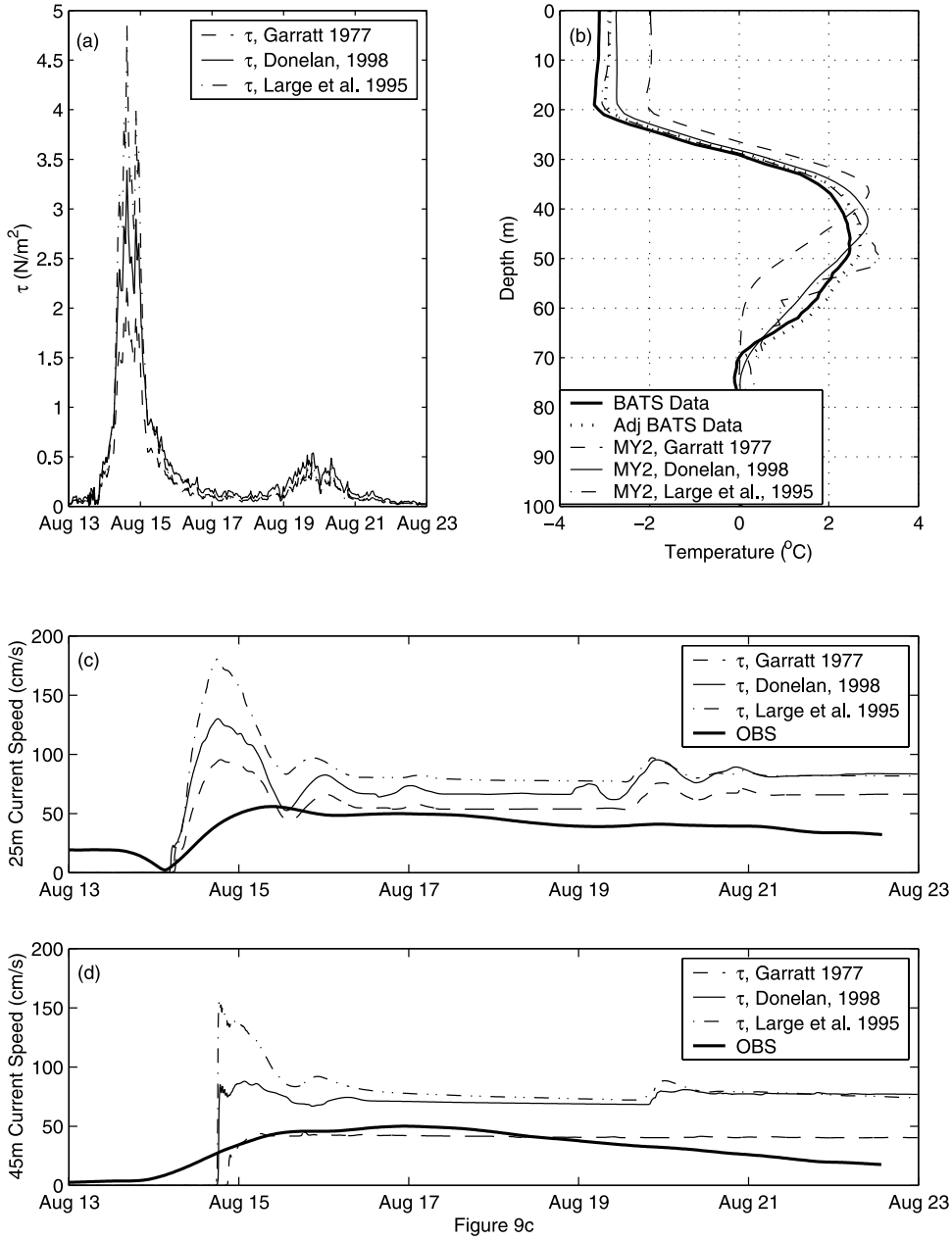

Figure 9c. (a) Wind stress time series used to force the MY2 model following *Garratt* [1977], *Donelan et al.* [1997], and *Large et al.* [1995]. (b) Simulated and measured profiles of temperature change in the upper 100 m of water for the three wind stress forcing cases indicated in (a). (c) Simulated and measured current speed at 25 m for the three wind stress forcing cases indicated in (a). (d) Simulated and measured current speed at 45 m for the three wind stress forcing cases indicated in (a).

poststorm current amplitudes as much as for case III, which used the measured direction (Figure 11). For the case of CCW wind rotation, the analogous difference was larger (~30 cm/s for both KPP and MY2 models). Apparently, this results because the strength and phase of the initial currents are more important when the transfer of wind energy to the currents during the storm is less efficient.

9. Discussion

[43] One-dimensional models cannot be expected to simulate all features of a response that has significant three-dimensional components. Nevertheless, the models should simulate locally generated near-inertial mixed layer currents and entrainment and shear driven mixing at the base of the mixed layer. There are several reasons for the use of one-dimensional models in this study: (1) our observations were collected at a site located approximately in the center of the cooling wake where advective effects may have been relatively less important, (2) scaling analysis [*Dickey et al.*, 1998a] suggests that the response to Hurricane Felix can be described to first order as a one-dimensional response (relative to slower moving storms), and (3) our wind and heat flux forcing measurements were local, and therefore

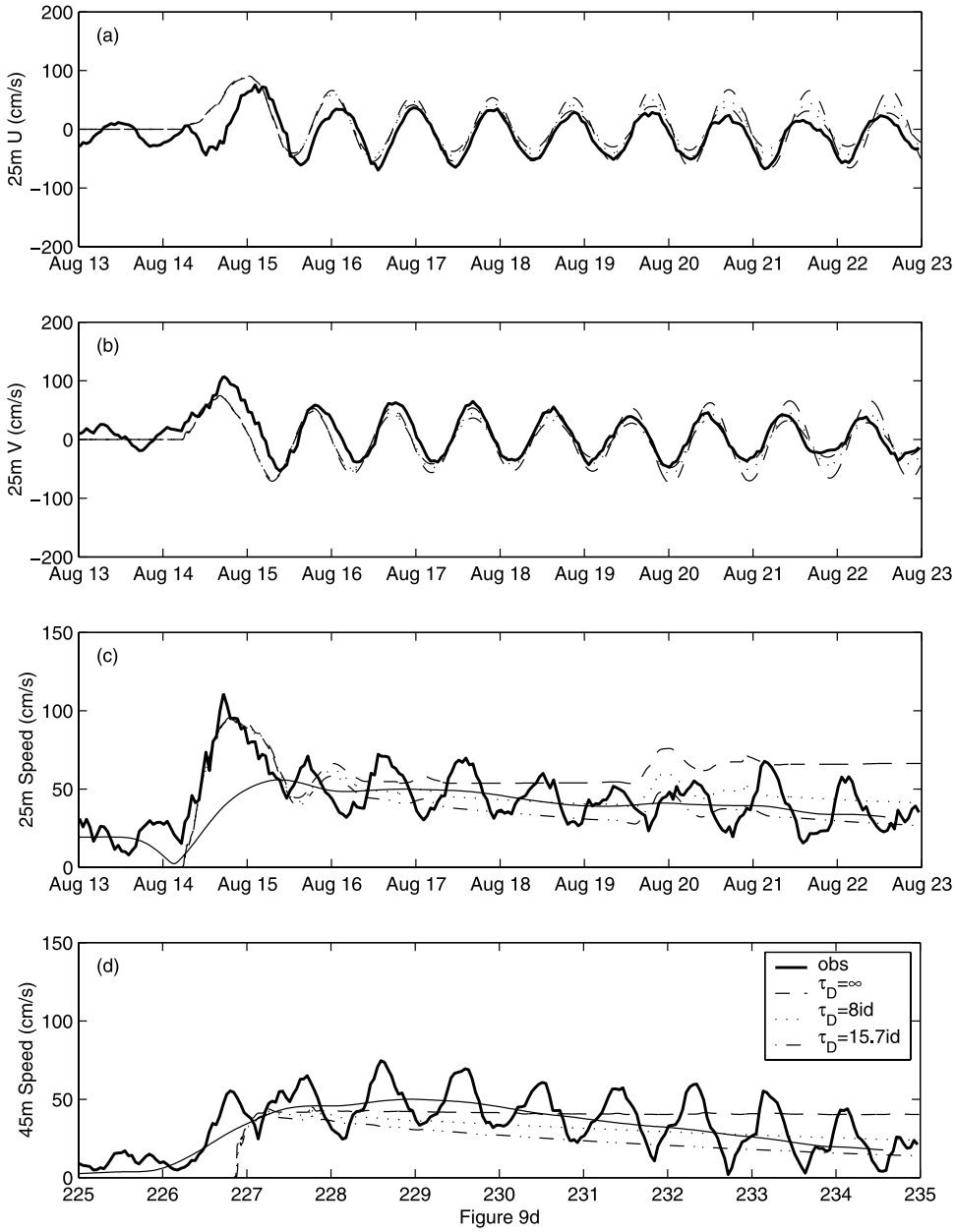

Figure 9d. (a) Simulated east current components at 25 m for three imposed decay timescales: $\tau_D = \infty$ (no decay), 8 inertial days, and 15.7 inertial days. Decay timescales are indicated on (d) (smooth solid line is complex demodulated amplitude of current). (b) Same as (a), but for north current components. (c) Current speeds at 25m for same simulations and observations. (d) Same as (c) but at 45 m.

were appropriate for this study. The models were all able to simulate the observed response qualitatively. However, there are significant quantitative differences among model simulations and with the observations. To this end, model skill is addressed in section 7. The focus of this discussion centers on the roles and efficacies of specific model features and parameterizations for predicting the response, thereby addressing the other main objectives of this paper.

[44] A distinctive component of the KPP model is gradient Richardson number (R_{gKPP}) instability mixing due to resolved shear. This feature allows for an increase in interior eddy viscosities when shear at the base of the mixed layer is relatively high (i.e., when local Richardson numbers (R_{gKPP}) are below a prescribed value). The matching condition for the diffusivity and viscosity profiles at the boundary layer depth implies that this will also affect (by increasing) diffusivities and viscosities just above the interior region. This can act to smooth the shear gradient between the mixed layer and the thermocline (i.e., working just below the planetary boundary layer; see equation (6) for definition of planetary boundary layer). In this way, the provision for gradient Richardson number (R_{gKPP}) instability mixing affects mixing directly by increasing diffusivities and viscosities in the interior, and indirectly by allowing for a deepening of the boundary layer. Although *Large et al.* [1994] report that mixing in the interior of this type was of

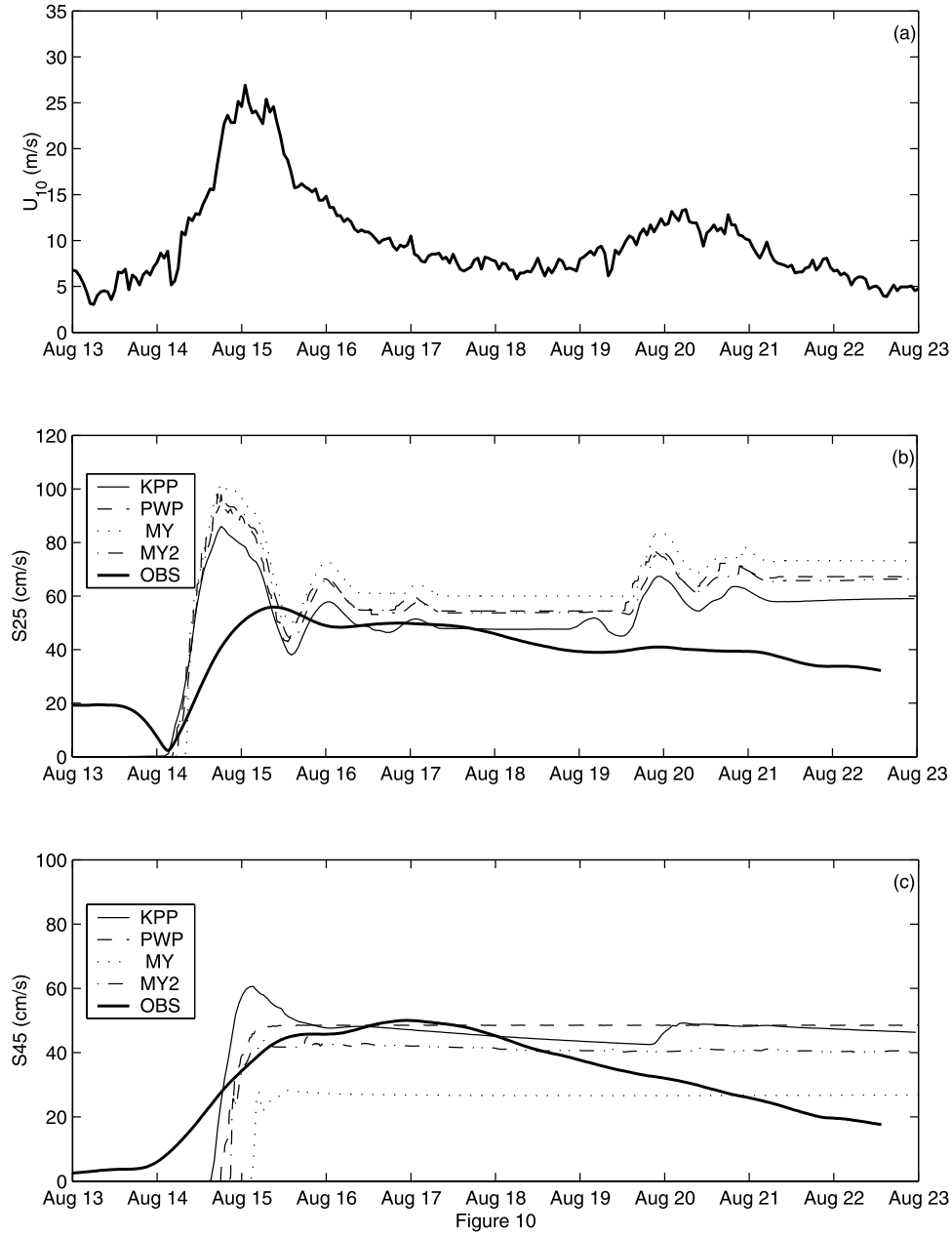

Figure 10. (a) Plot of U_{10} used for case I forcing. (b) Complex demodulated inertial current amplitude and modeled current speeds for KPP, PWP, MY, and MY2 simulations at 25 m. (c) Same as (b), but at 45 m.

Table 3. Average of Highest 25 m Speeds (i.e., of Currents Higher Than 70% of the Maximum Value of the Model-Specific 25 m Currents) During the Storm Residence Period and Average Speed During the Poststorm Period (17–19 August) at 25 and 45 m for Observations and the MY, MY2, PWP, and KPP Model Simulations

	Storm Forced Period[a]	Poststorm Period (17–19 August)	
	25 m	25 m	45 m
OBS	93.8 ± 10	45 ± 13	45 ± 13
D(t, 25 m)	N/A	45 ± 4	45 ± 4
MY	92 ± 8	61 ± 1	26 ± 0
MY2	86 ± 8	54 ± 1	41 ± 1
PWP	86 ± 7	55 ± 1	49 ± 0
KPP	76 ± 7	48 ± 1	45 ± 1

[a]Storm-forced period defined separately for each model as the time during 70% percentile of maxiumum currents. Reported errors are 1 standard deviation from the mean.

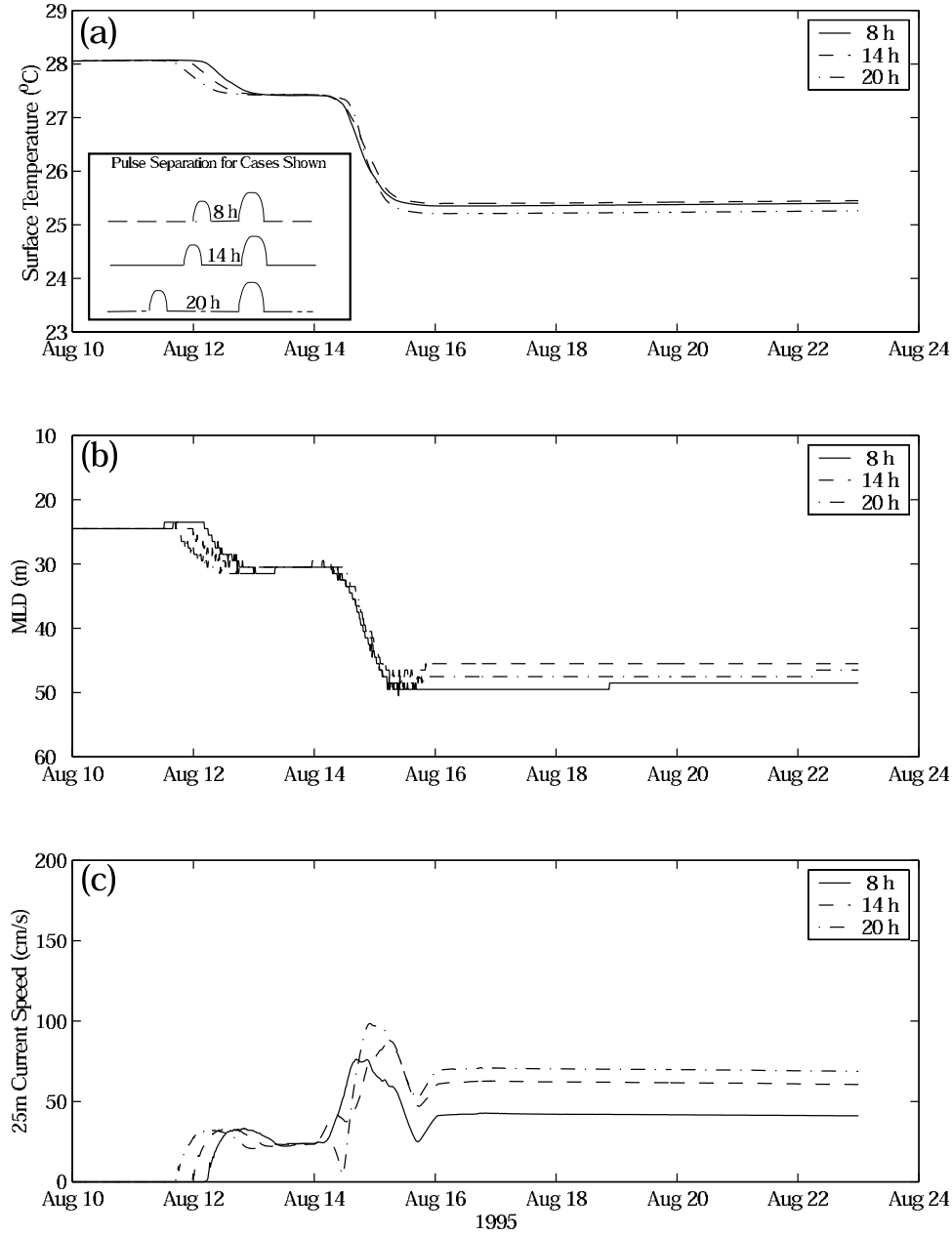

Figure 11. All results shown are from the KPP model simulations. (a) Sea surface temperature for three separate pulsing experiments: separation between pulses of 8, 14, and 20 hours. (b) Mixed layer depth (based on 0.5°C criterion) for above three cases. (c) Current speed at 25 m corresponding to above three cases. Wind-forcing direction and pulse separation are indicated in (a).

minor importance for an (idealized) simulation forced with a constant wind stress and no heat fluxes, the high current shear observed in response to Hurricane Felix suggests that this mixing parameterization should be more important for this situation. When a simulation using the KPP model was done with this type of interior mixing turned off (denoted as a KPP_b simulation), the boundary layer shoaled slightly and vertical mixing was dramatically reduced. For this simulation, sea surface cooling was ~1.2°C (as opposed to ~3.0°C; Figures 13a and 13c), the mixed layer depth was ~38 m (7 m shallower than that obtained using KPP), the currents fell to zero by a depth of 45 m (as opposed to ~65 m; Figures 13b and 13d), and the heat lost from the upper 29 m was 110.6 MJ/m^2 (less than half that predicted by KPP). This behavior results from decreased momentum eddy viscosity in the interior, which corresponds to decreases in shear production near the base of the boundary layer (~40 m), and buoyancy production. These results illustrate that one purpose served by local Richardson number mixing (R_{gKPP}) in the KPP interior is the same as the function of gradient mixing in the PWP; namely, smoothing of the vertical temperature (density) profile below the mixed layer. However, the significant difference between the two mixing schemes is that in the KPP, smoothing of the profile results in deeper penetration of the planetary boundary layer. We note here that this study

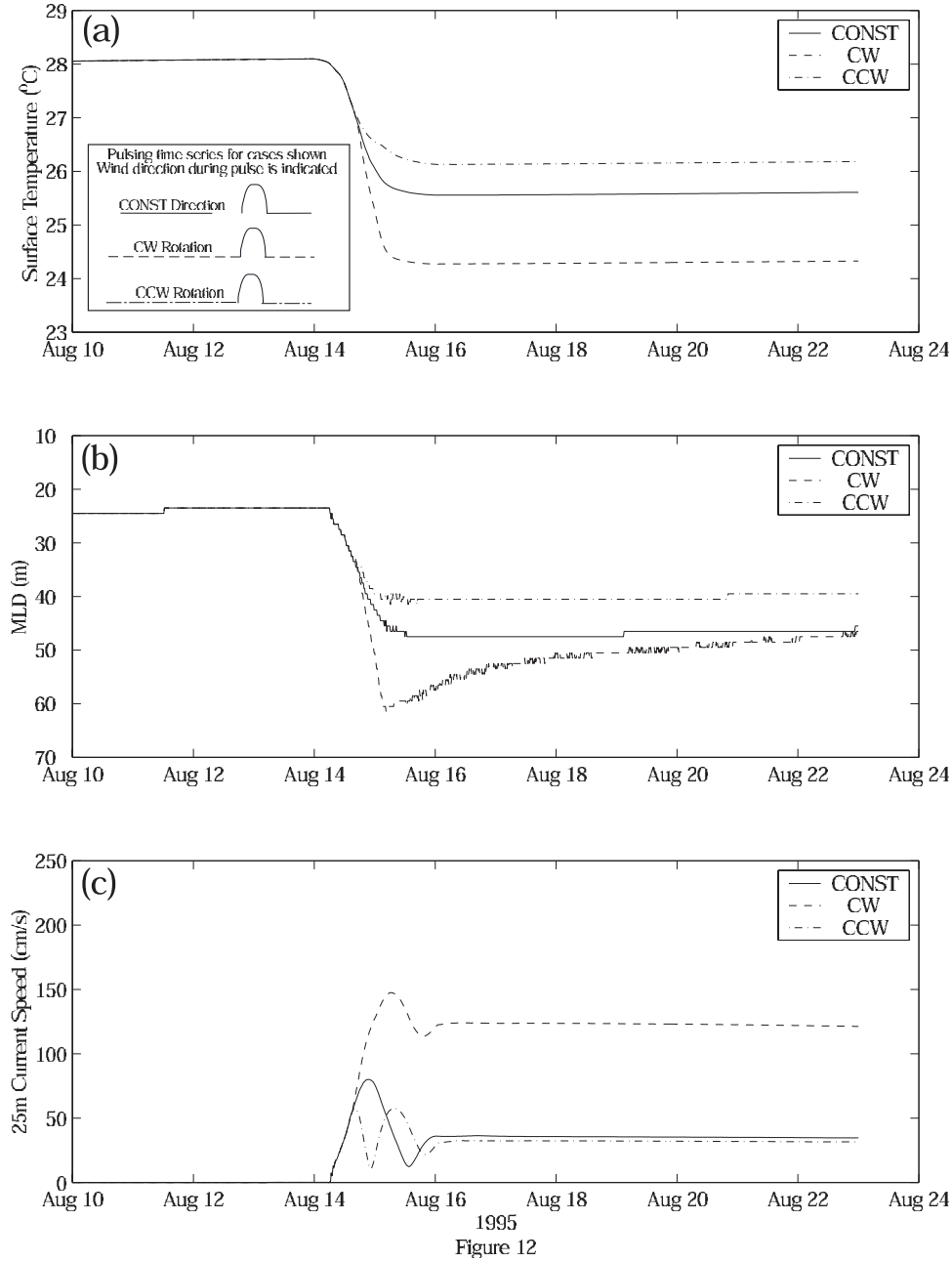

Figure 12

Figure 12. All results shown are from the KPP model simulations. (a) Sea surface temperature for CW and CCW rotation of winds, as well as for constant direction. (b) The 0.5°C mixed layer depth for above three cases. (c) The 25 m current speeds for above three cases. Wind-forcing direction and pulse separation for three cases shown is indicated in (a).

considers what is almost entirely a wind driven response and that the convective mixing parameterization in the KPP could be more important for other, more buoyancy driven events.

[45] The PWP simulates mixing due to free convection, mixed layer entrainment, and local shear instabilities. The model can be easily run with one or two of these processes separately (with two or one of the other processes turned off; Figure 14). Clearly, within the framework of the PWP, free convection alone accounts for very little heat exchange or mixed layer deepening with the result that current values are high near the surface and kinetic energy is confined to a thin layer (Figures 14c–14d). In the absence of local Richardson number (R_{gPWP}) instability mixing, the model predicts a decrease in sea surface temperature of 1.7°C (as opposed to 2.2°C for the full PWP; Figures 14a and 14e), and the amount of depth-integrated heat lost from the upper 29 m (DIH_{0-29}) was about 75% of the value calculated for the full PWP. Current energy was also confined to the upper 45 m of water for this simulation (Figure 14f). With mixed layer entrainment turned off, the simulated and full model responses are nearly identical for the measure of temperature (Figures 14a and 14g), but in this version of the model mixed layer deepening is set by free convection after sunset

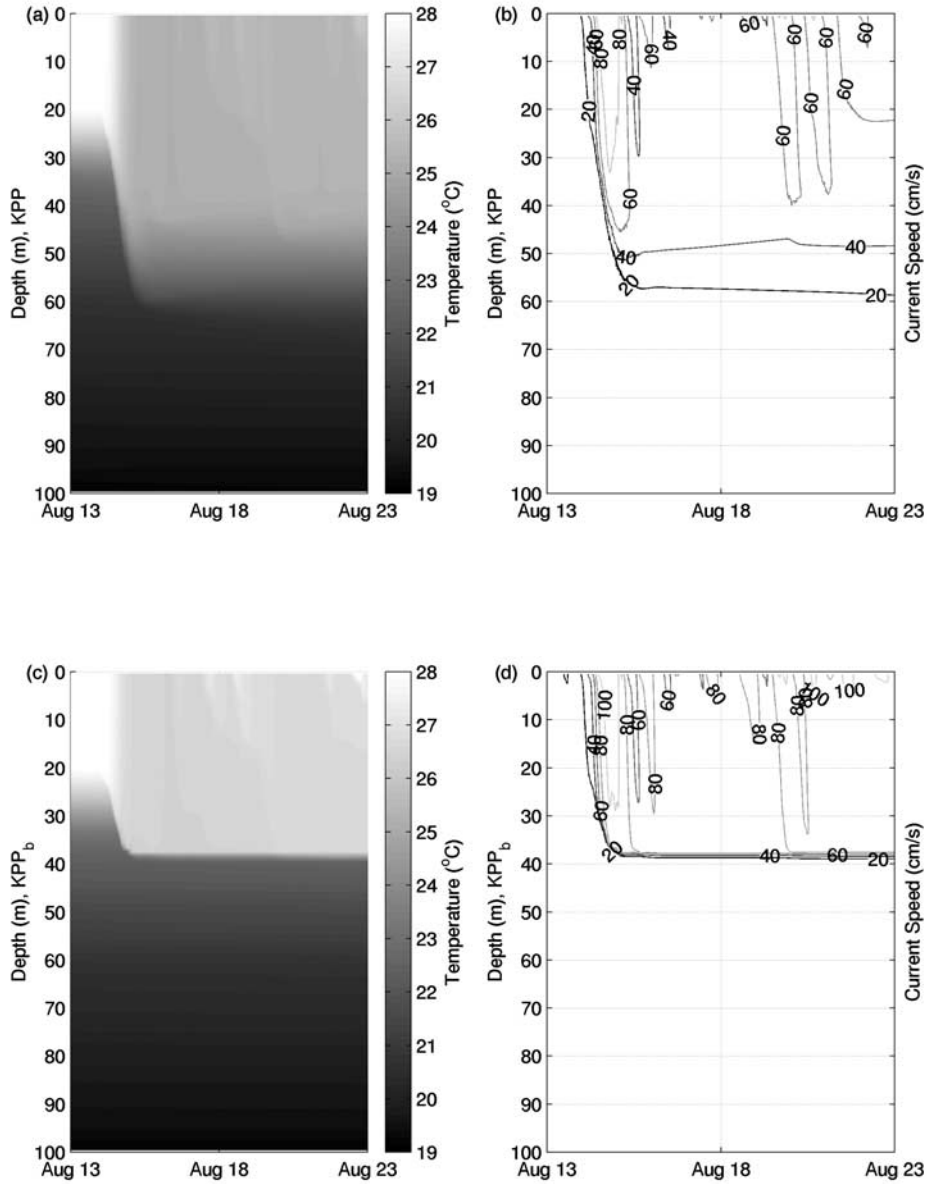

Figure 13. KPP simulation with and without (KPP_b) and the inclusion of mixing in the interior for case I forcing and initialization. All plots are for the time period 13–23 August and the depth interval 0–100 m. (a) Temperature contour for the full KPP. (b) Horizontal current contour for full KPP. Current contour labels have intervals of 20 cm/s. (c) Same as (a), but for KPP_b simulation. (d) Same as (b), but for KPP_b simulation.

[*Price et al.*, 1986], and so is not realistic (it cannot form a mixed layer from wind mixing alone). Therefore, by treating the model as an embellished version of a bulk stability model with an additional provision for smoothing of the temperature profile at the base of the mixed layer, we conclude that most of the mixed layer deepening in the PWP can be attributed to mixed layer entrainment, with the remainder due to local Richardson number (R_{gPWP}) instability mixing. Notably, changing the critical bulk Richardson number for mixed layer entrainment (R_{bPWP}) from its default value of 0.65 to a value of 0.70 only resulted in minor changes in the temperature response (results not shown).

[46] The MY2 model predicted a greater depth of vertical mixing and sea surface cooling than the MY model (Figure 15). The turbulent kinetic energy equation for both the MY and MY2 models is given by

$$\frac{D}{Dt}\left(\frac{q^2}{2}\right) - \frac{\partial}{\partial z}\left[lqS_q\frac{\partial}{\partial z}\left(\frac{q^2}{2}\right)\right] = P_s + P_b - \varepsilon \tag{8}$$

where

$$P_s = K_m\left[\left(\frac{\partial U}{\partial z}\right)^2 + \left(\frac{\partial V}{\partial z}\right)^2\right] \tag{9a}$$

$$P_b = \beta g K_h\left[\frac{\partial T}{\partial z}\right] \tag{9b}$$

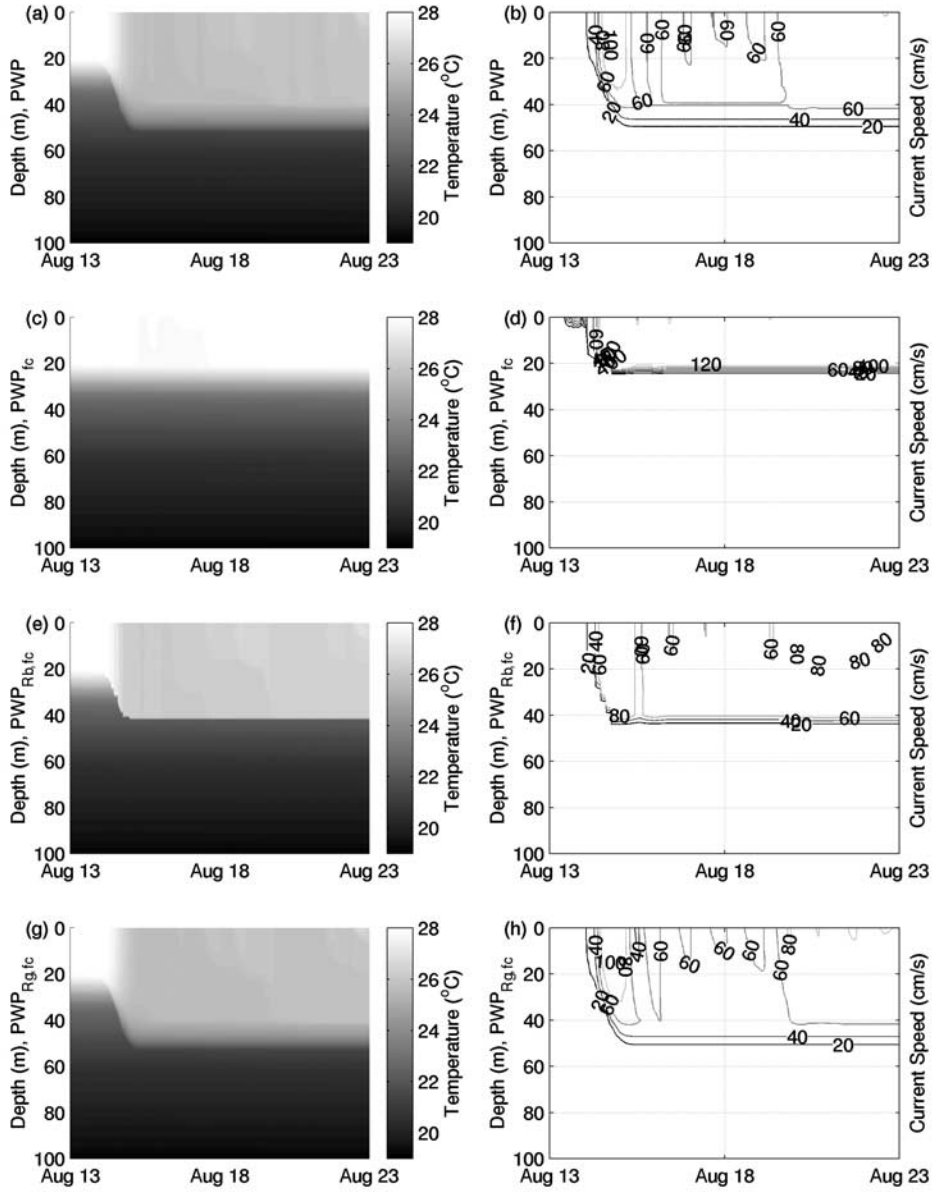

Figure 14. Temperature and horizontal current speed contours generated from different versions of the PWP with case I forcing and initialization. All plots are for the time period 13–23 August and the depth interval 0–100 m. Horizontal current speed contours are in intervals of 20 cm/s. (a) Temperature, full PWP. (b) Horizontal current contour for full PWP. (c) Temperature evolution for PWP with only free convection. Mixed layer entrainment and local shear instability mixing were turned off. (d) Horizontal current speed contour for same case as (c). (e) Temperature evolution for PWP with only mixed layer entrainment and free convection. (f) Horizontal current speed contour for same case as (e). (g) Temperature evolution for PWP with local shear instability mixing and free convection. (h) Horizontal current speed components for same case as (g).

$$K_m = lqS_M \tag{10a}$$

$$K_h = lqS_H \tag{10b}$$

The terms in equation (8) are from left to right: time rate of change of turbulent kinetic energy, diffusion of turbulent kinetic energy, shear production, buoyancy production, and dissipation rate of turbulent kinetic energy. Also, S_q, S_M and S_H are stability similarity functions.

[47] Equation (8) stipulates that a decrease in dissipation rate results in increases in turbulent kinetic energy. Further, Equations (9a)–(9b) and (10a)–(10b) show that buoyancy and shear production are proportional to q, so an increase in turbulent kinetic energy results in increases in P_s and P_b which ultimately leads to enhanced vertical mixing and lower posthurricane sea surface temperatures in the MY2 model.

[48] We stress that although the *Mellor* [2001] modification promotes similar behavior to that obtained through the

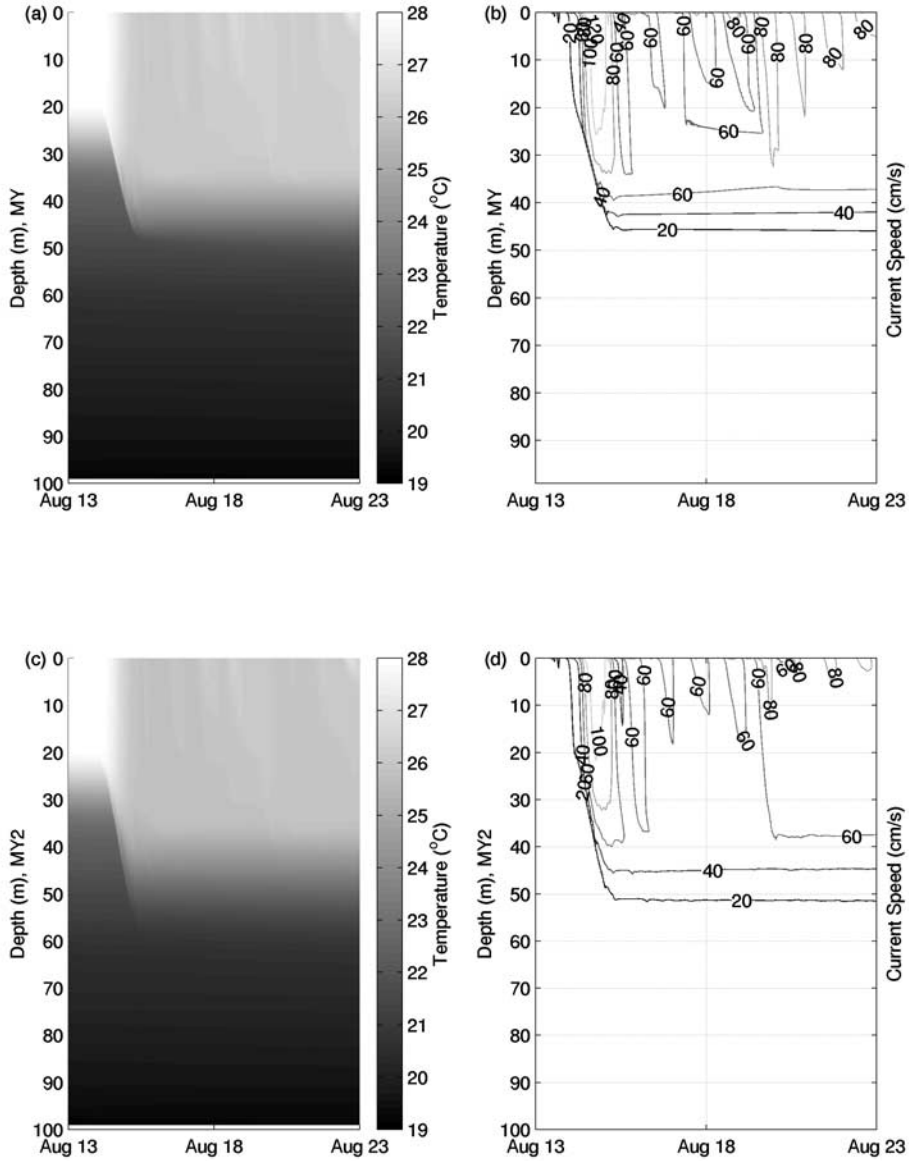

Figure 15. Temperature and horizontal current speed contours for the MY and MY2 for case I forcing and initialization. All plots are for the time period 13–23 August and the depth interval 0–100 m. Horizontal current speed contours are in intervals of 20 cm/s. (a) Temperature contour for MY. (b) Horizontal current speed contour for MY. (c) Temperature contour for MY2. (d) Horizontal current speed contours for the MY2.

inclusion of Richardson number dependent mixing in the interior [*Kantha and Clayson*, 1994; *Large et al*, 1994], the two approaches are fundamentally different. The interior mixing parameterized by *Large et al.* [1994] and applied to the MY model by *Kantha and Clayson* [1994] results in increases in thermocline viscosity when Richardson instabilities are present. On the other hand, increases in viscosity in the MY2 result indirectly from a reduction in the dissipation rate.

10. Conclusions

[49] Overall, the model results show that for temperature and currents, the observed response can be partly explained as a one-dimensional phenomenon, but also that three-dimensional processes such as propagation of internal gravity waves and inertial pumping must have contributed to the cooling response. There were significant differences in model responses. In particular, the KPP model predicted sea surface cooling, mixed layer currents, and the maximum depth of cooling closer to the observations than any of the other models. This was shown to be partly because of a special parameterization for gradient Richardson number (R_{gKPP}) shear instability mixing in response to resolved shear in the interior. The MY2 model predicted enhanced sea surface cooling over the MY model, because of a decrease in dissipation under stable conditions when internal gravity waves are

likely to be present, which translates to higher diffusivities. For the PWP model, mixing was mainly influenced by bulk Richardson mixing (R_{bPWP}), a parameterization of entrainment.

[50] Reliable calculations of the wind stress, and measurements of the wind speed and direction, were quite important for the success of the simulations; in a general sense, the wind scales the strength of local physical mixing processes. Specific processes that may have affected the appropriate wind stress formulation could include a wave distortion effect due to the low height of the sensor, the presence of cross-wind or counterwind swell, or the presence of young waves during the highest winds. Calculation of wind stress is highly controversial, especially under high winds. The results of this study support the need for more data at high wind speeds. Toward this end, we would like to mount wave sensors on the BTM mooring, so that sea states can be examined using directional wave spectra under a variety of wind conditions, hopefully during another hurricane. Sensitivity experiments suggest that the phase of preexisting near-inertial currents likely affected the magnitude of poststorm currents slightly, and that there was probably not a significant resonant response due to clockwise near-inertial rotation of the wind stress during the highest winds at our site.

Appendix A: Calculations

A1. Depth-Integrated Heat

[51] The depth integrated heat anomaly (DIH) was calculated over particular depth intervals [*Large et al.*, 1986] using the equation

$$DIH = \rho_o c_{pw} \int_{z_1}^{z_2} (T_{18}(z) - T_{10}(z))dz \tag{A1}$$

for vertical intervals where there was cooling ($[z_1,z_2]$ = [0,29]), warming ([29,70]), and no net change in temperature ([0,70]) due to the storm. The maximum depth of integration was chosen to be 70 m, the apparent maximum depth of penetration for vertical mixing. Here, T_{18} and T_{10} refer to the temperature profiles taken on 18 August and 10 August, respectively (Figure 3). Water density is ρ_o and c_{pw} is the specific heat of water ($\rho_o c_{pw}$ = 4.1 MJ/(°C m^3)). The reported error bars are ± one standard deviation from the mean temperature of 7 profiles taken on 18 August. These casts were collected in different areas, so deviations from the average of these profiles likely reflect lateral gradients and high frequency temporal variability as well as vertical variability in the temperature distribution. Variability in the 10 August temperature profile is unknown, because only one profile was obtained.

A2. Complex Demodulated Current Amplitude

[52] To obtain a time series of the inertial current amplitude, complex demodulation [*Bloomfield*, 1976] was performed using a formula presented by *Qi et al.* [1995]:

$$D(\tau) = \left(\frac{1}{2\Gamma}\right) \int_{\tau-\Gamma}^{\tau+\Gamma} W(\tau - t)S(t)e^{i\varpi t}dt \tag{A2}$$

where a triangular window was chosen for the weighting function W, S = U + iV is the complex velocity, and the frequency of demodulation ϖ was chosen to be 0.0455 cph instead of the local inertial frequency (f = 0.0439 cph at 31°N), so that we could integrate over an integral number of periods. The window length (2Γ) was chosen to be 2 demodulation periods (44 hours).

A3. Change in Inertial Kinetic Energy

[53] The inertial amplitudes calculated for 25 m were used to compute increases in average inertial kinetic energy density in the mixed layer ($\Delta IKE_{25}(\tau)$) using the following equations:

$$IKE_{25}(\tau) = \frac{1}{2}\rho(\tau)h(\tau)D(\tau, 25m)^2, \tag{A3}$$

$$h(\tau) = \left\{ \begin{array}{ll} 23 & \tau \le \text{August14} \\ 46 & \tau > \text{August14} \end{array} \right\} \tag{A4}$$

$$\rho(\tau) = \left\{ \begin{array}{ll} 1023.6 & \tau \le \text{August14} \\ 1024.7 & \tau > \text{August14} \end{array} \right\} \tag{A5}$$

$$\Delta IKE_{25} = \frac{\int_{t2}^{t3} IKE_{25}(\tau)d\tau}{\int_{t2}^{t3} d\tau} - \frac{\int_{t0}^{t1} IKE_{25}(\tau)d\tau}{\int_{t0}^{t1} d\tau} \tag{A6}$$

In these equations, D(τ, 25 m) is the amplitude of the complex demodulated velocity at 25 m, h is the mixed layer depth, τ is time, and the integrals are calculated for the prehurricane ($[t_0, t_1]$ = [11–14 August]) and posthurricane ($[t_2, t_3]$ = [17–19 August]) periods. Note that the mixed layer depths were nearly constant during these respective periods. The density was calculated using temperature from the 10 and 18 August profiles and the UNESCO polynomial [*Fofonoff and Millard*, 1983; *Millero et al.*, 1980].

Appendix B: Wind Stress and Heat Flux Forcing

B1. Wind Stress Forcing

[54] Wind speed and direction were measured at $z_o \sim 4.2$ m above sea level (Figure 2). For cases I and II, the winds were adjusted to 10 m assuming a logarithmic wind profile and neutral stability [*Large et al.*, 1995] by solving the following system of equations for U_{10}:

$$U_{10} = U(z_o) + \frac{u_*}{\kappa}\left[\ln\left(\frac{10}{z_0}\right)\right] \tag{B1}$$

$$u_*^2 = 10^{-3}\left[2.717U_{10} + 0.142U_{10}^2 + 0.0764U_{10}^3\right] \tag{B2}$$

where z_o = 4.2 m is the height of the wind sensor, $U(z_o)$ is the uncorrected wind measured by the sensor at height z_o, u_* is the friction velocity (parameterized in equation (B2) following E. Vera (unpublished manuscript, 1983)), κ = 0.4 is von Karman's constant, and ρ_a is air density. Note that when this

cubic equation was solved using the drag coefficients of *Large and Pond* [1981] and *Garratt* [1977] (instead of the parameterization used by Vera) the variation in U_{10} was less than 1% over the wind speed range 0–45 m/s. The east and north components of wind stress were calculated using the bulk formulas [*Martin*, 1982; *Doney*, 1996]:

$$\tau_x = -\rho_a c_d U_{10}^2 \sin\theta \tag{B3}$$

$$\tau_y = -\rho_a c_d U_{10}^2 \cos\theta \tag{B4}$$

where τ_o is the wind stress at 10 m corrected for atmospheric stability, c_d is formulated as a function of wind speed, θ is the direction from which the wind comes and is measured clockwise from the north. For case I, the drag coefficient form of *Garratt* [1977] was used:

$$c_d = 10^{-3}*(0.75 + 0.067U_{10}), \qquad 0 < U_{10} < 21\text{m s}^{-1} \tag{B5}$$

For case II, the 10 m winds (U_{10}) were adjusted for wave distortion by applying the linear relation presented by *Large et al.* [1995] for a sensor mounted at 4.5 m (they did not report a correction for a sensor mounted at 4.2 m):

$$U_{10w} = \left\{ \begin{array}{ll} U_{10}, & U_{10} \le 9.05\text{m s}^{-1} \\ 1.53*U_{10} - 4.80, & U_{10} > 9.05\text{m s}^{-1} \end{array} \right\} \tag{B6}$$

and the drag coefficient form of *Large and Pond* [1981] was adopted:

$$c_d = \left\{ \begin{array}{ll} 1.2*10^{-3}, & 0 \le U_{10w} < 11\text{m s}^{-1} \\ (0.49 + 0.65U_{10w})*10^{-3} & 11 \le U_{10w} \le 25\text{m s}^{-1} \end{array} \right\} \tag{B7}$$

Two important points regarding the drag coefficients applied for cases I and II (equations (B5) and (B7)) are (1) the *Garratt* [1977] drag coefficient parameterization produces wind stress magnitudes that are an average of 15.1% higher than those computed using the *Large and Pond* [1981] parameterization over the range of 10 m wind from 15–35 m/s (covering the range of highest winds observed), and (2) they are reported to be valid for 10 m adjusted winds of up to 21 m/s (equation (B5)) and 25 m/s (equation (B7)) respectively, which are lower than the maximum 10 m adjusted winds during Hurricane Felix (27 m/s).

B2. Surface Heat Flux Forcing

[55] The net heat flux budget at the surface was formulated using the standard air-sea transfer equations presented by *Doney* [1996]:

$$Q^{net} = Q_{sen} + Q_{lat} + Q_{lw}^{net} + Q_{sw}^{net}, \tag{B8}$$

$$Q_{sen} = \rho_a c_{pa} C_H U_{10}(T_a - T_s) \tag{B9}$$

$$Q_{lat} = \rho_a L_v C_E U_{10}(q_a - q_s) \tag{B10}$$

$$Q_{lw}^{net} = -\varepsilon_o \sigma \left(T_a^4 \left[0.39 - 0.05 e_a^{0.5}\right] F(C) + 4T_a^3 [T_s - T_a] \right) \tag{B11}$$

$$F(C) = 1 - 0.63C \tag{B12}$$

$$\log_{10} e_a(T_s) = (0.7859 + 0.03477T_s)/(1 + 0.00412T_s) \tag{B13}$$

where Q_{sen} is sensible heat flux, Q_{lat} is latent heat flux, Q_{lw}^{net} is net longwave radiation, and Q_{sw}^{net} is net shortwave insolation. Time series used in these equations are wind speed at 10 m as calculated for intermediate winds as described in this appendix (U_{10}), air temperature (T_a) from NCEP/NCAR reanalysis data interpolated for coordinates near the mooring [*Doney et al.*, 1998], sea surface temperature based on BTM measurements at 25 m (T_s), relative humidity (used in calculation of specific humidity at the standard level and at the sea surface, q_a and q_s, respectively) based on a climatological average, and BTM measurements of downwelling solar irradiance (Q_{sw}^{net}; also used to estimate cloud cover C). Saturation vapor pressure (equation (B13)) and specific humidity were calculated using equation A4.5 and the equations presented in chapter 3.1 of *Gill* [1984]. Constants were the specific heat of air at constant pressure (c_{pa}), latent heat of vaporization (L_v), bulk transfer coefficients (C_H and C_E), emissivity of the Earth's surface (ε_o), and the Stefan Boltzmann constant (σ), and were set as follows: $\rho_a = 1.22$ kg/m^3, $c_{pa} = 1003$ J/(kgK), $C_H = 9.7 \times 10^{-4}$ (no units), $C_E = 1.5 \times 10^{-3}$ (no units), $L_v = 2.45 \times 10^6$ J/kg, $\varepsilon_o = 0.985$ (no units), and $\sigma = 5.7 \times 10^{-8}$ W/(m^{2}K^4). Descriptions of and explanations for our estimates of Q_{sw}^{net}, T_s, and C are provided below.

[56] Because direct measurements of shortwave insolation (Q_{sw}^{net}) were unavailable, this quantity was estimated by applying an empirically derived linear fit between measured surface shortwave and PAR for a later deployment (BTM Deployment #7) to estimates of the integral of spectral PAR (λ = 412, 443, 490, 510, 555, 665, and 683 nm). This was the only other spring/summer deployment during which the pyranometer and PAR sensors were deployed concurrently. The squared coefficient of correlation between these records (r^2) was 0.95 with a slope of 2.1348 and an intercept of −2.486. Interestingly, this corresponds to a 46.9% contribution of PAR to the total solar energy, which is in good agreement with the fraction of visible energy obtained from integrating the visible portion of the normalized Tanre spectrum (46%; courtesy of Carter Ohlmann) for a clear day. The quality of Deployment 7 data was compared with (and shown to be favorable with) BBOP estimates of integrated PAR [*Dickey et al.*, 2001].

[57] The *Reed* [1977] formula for insolation was used to calculate cloud fraction (C; equations (B11)–(B12)):

$$Q_{sw}^{net} = S_o T_r \mu_o^D (1 - 0.632C + 0.0019m) \tag{B14}$$

In the above equation, S_0 is the solar constant (1367 W/m^2), T_r is the atmospheric transmission (assumed to be 0.7), μ_0^D is the daily averaged cosine of the solar zenith angle, and m is the solar altitude in degrees.

[58] The 25 m temperature record was chosen to represent sea surface temperature in heat flux equations (B8)–(B11) and (B13) (either directly or indirectly). This likely introduced a bias in the net heat flux calculations for the one day period just prior to the passage of Felix, but is probably not

critical for such a short simulation and under such extreme wind conditions (where heat flux is not the dominant forcing factor). During the post-Felix period, the 25 m record was clearly from the mixed layer, and probably a few tenths of a degree different from the actual sea surface temperature at most.

Notation

Symbol	Description
B	constant in MY2 model, 16.6, no units.
C	cloud fraction, no units.
C_E, C_H	bulk transfer coefficients, 1.5×10^{-3}, 9.7×10^{-4}, respectively, no units.
c_d	velocity dependent drag coefficient, no units.
c_p	phase speed of the waves at the spectral peak, m/s.
c_{pa}	specific heat of air at constant pressure, 1003 J/(kgK).
c_{pw}	specific heat of water at constant pressure, 4004 J/(kgK).
$D(\tau)$	complex demodulated current amplitude, cm/s.
DIH	net depth integrated heat anomaly, J/m^2.
e_a	vapor pressure at 10 m above the sea surface, N/m^2.
G_H, G_{Hc}	MY2 variable (proportional to Richardson number), and MY2 empirical constant, no units.
g	acceleration due to gravity, 9.81 m/s^2.
h	mixed layer depth, m.
$IKE_{25}(t)$	average depth integrated KE stored in ML, J/m^2.
L_v	latent heat of vaporization of water, 2.45×10^6 J/kg.
l	turbulent length scale, m.
m	solar altitude, degrees.
P_b, P_s	buoyancy and shear production, J/(kgs).
Q_{lat}	latent heat flux across sea surface, positive into ocean, W/m^2.
Q_{net}	net total heat flux across sea surface, positive into the ocean, W/m^2.
Q_{net}^{lw}	net longwave heat flux across sea surface, positive into the ocean, W/m^2.
Q_{net}^{sw}	net shortwave heat flux across sea surface, positive into the ocean, W/m^2.
Q_{sen}	sensible heat flux across sea surface, positive into the ocean, W/m^2.
q^2	twice the turbulent kinetic energy per unit mass, J/kg.
q_a	specific humidity at 10 m height above sea surface, no units.
q_s	specific humidity just above the sea surface, no units.
r^2	squared coefficient of correlation, no units.
R_{gc}, R_{ic}	critical bulk and gradient Richardson numbers for KPP, no units.
R_{bKPP}, R_{bPWP}	bulk Richardson numbers for indicated model, no units.
R_{gMY}, R_{gMY2}	gradient Richardson numbers for indicated model, no units.
R_{gKPP}, R_{gPWP}	gradient Richardson numbers for indicated model, no units.
R_{io}	constant in KPP model, 0.7, no units.
S_H, S_M, S_q	stability similarity function, no units.
S	complex horizontal current speed, cm/s.
S_o	solar constant, 1367 W/m^2.
S_p	horizontal current amplitude, m/s.
T	time-averaged water temperature, °C.
T_a	air temperature at 10 m height above the sea surface, °C.
T_r	atmospheric transmission, 0.7, no units.
T_s	air temperature just above the sea surface, °C.
u_*	friction velocity, m/s.
U,V	time-averaged east and north currents, cm/s.
U_{10}	wind speed at 10 m, m/s.
U_{10w}	wind speed at 10 m corrected for wave distortion, m/s.
W	triangular window function (complex demodulation), no units.
z	depth, positive downward in KPP and PWP, but upward in MY and MY2, m.
z_o	height of wind sensor above sea surface, 4.2 m.
ΔIKE_{25}	average change in-depth-integrated KE in ML, J/m^2
β	thermal expansion coefficient, (1/°C).
ε	turbulent kinetic energy dissipation rate, J/(kgs).
ε_o	emissivity of the Earth's surface, 0.985, no units.
κ	von Karman's constant, 0.4, no units.
Γ	half window length for complex demodulation, s.
μ_D^o	daily averaged cosine of the solar zenith angle, no units.
θ	direction of wind measured clockwise from north, degrees.
ρ_a, ρ_o	mean density of air, 1.22 kg/m^3, and of seawater, 1024 kg/m^3.
ρ	density of seawater, kg/m^3.
σ	Stefan-Boltzmann constant, 5.7×10^{-8} W/(m^{2}K^4).
τ	time, Julian day.
τ_x, τ_y	east and north components of wind stress, N/m^2.
υ, υ_o	eddy viscosity, m^2/s, and critical eddy viscosity, 5.0×10^{-3}, m^2/s.
ϖ	frequency of complex demodulation, 1/s.

[59] **Acknowledgments.** The BTM has been supported by the National Science Foundation's Ocean Technology and Interdisciplinary Coordination Program, the Chemical Oceanography Program, and the Oceanographic Instrumentation and Technical Service Program (TD: OCE-9627281, OCE-9730471, OCE-9819477), the Office of Naval Research/National Ocean Partnership Program (TD: N40000149810803), the Office of Naval Research Ocean Engineering and Marine Systems Program (Dan Frye: N00014-96-1-0028), National Aeronautics and Space Administration SIMBIOS Program (TD: NAGW-3949, NAS5-97127), SeaWiFS grant W-19,223 (SCD), and the University of California, Santa Barbara (to T. Dickey, UCSB). Funds were also provided by BTM collaborators for mooring operations. NCAR is sponsored by the National Science Foundation. We would like to extend special thanks to colleagues at the Ocean Physics Laboratory who have made the BTM project possible: engineers Derek Manov, Dave Sigurdson, and Frank Spada; post-doctoral

fellows Joe McNeil and Laura Dobeck; visiting scholars Songnian Jiang and Xiaobing Zheng; computer specialist Charles Kiedman; and several undergraduate assistants. Gregory Crawford gave advice about the wind stress time series and Libe Washburn helped with time series analysis. Finally, thanks go to Bill Large and two anonymous reviewers who provided several comments and suggestions that have improved the paper. Norm Nelson provided a time series of composite AVHRR satellite imagery near the BTM. Dave Siegel and Margaret O'Brien shared temperature profile data collected as part of the BBOP program. Additional temperature profile data were provided by the BATS and Hydrostation S programs courtesy of Rob Johnson. Dan Frye and John Kemp are thanked for their collaborations with our group on the BTM since its inception in 1994. We would like to thank the captain and crew of the R/V Weatherbird II for their assistance at sea.

References

Bloomfield, P., *Fourier Analysis of Time Series: An Introduction*, pp. 118–150, John Wiley, New York, New York, 1976.

Brink, K. H., Observations of the response of thermocline currents to a hurricane, *J. Phys. Oceanogr.*, *19*, 1017–1022, 1989.

Brooks, D. A., The wake of Hurricane Allen in the western Gulf of Mexico, *J. Phys. Oceanogr.*, *13*, 117–129, 1983.

Crawford, G. B., and W. G. Large, A numerical investigation of resonant inertial response of the ocean to wind forcing, *J. Phys. Oceanogr.*, *26*, 873–891, 1996.

D'Asaro, E. A., Upper-ocean inertial currents forced by a strong storm, part II, Modeling, *J. Phys. Oceanogr.*, *25*, 2937–2952, 1995a.

D'Asaro, E. A., Upper-ocean inertial currents forced by a strong storm, part III, Interaction of inertial currents and mesoscale eddies, *J. Phys. Oceanogr.*, *25*, 2953–2958, 1995b.

D'Asaro, E. A., C. C. Eriksen, M. D. Levine, P. Niiler, C. A. Paulson, and P. Van Meurs, Upper-ocean inertial currents forced by a strong storm, part I, Data and comparisons with linear theory, *J. Phys. Oceanogr.*, *25*, 2909–2936, 1995.

Dickey, T. D., and G. L. Mellor, Decaying turbulence in neutral and stratified fluids, *J. Fluid Mech.*, *99*, 13–31, 1980.

Dickey, T. D., and J. J. Simpson, The influence of optical water type on the diurnal response of the upper ocean, *Tellus*, *35*, 142–154, 1983a.

Dickey, T. D., and J. J. Simpson, The sensitivity of upper ocean structure to time varying wind direction, *Geophys. Res. Lett.*, *10*, 133–136, 1983b.

Dickey, T. D., D. Frye, J. McNeil, D. Manov, N. Nelson, D. Sigurdson, H. Jannasch, D. Siegel, A. Michaels, and R. Johnson, Upper ocean temperature response to Hurricane Felix as measured by the Bermuda Testbed Mooring, *Mon. Weather Rev.*, *126*, 1195–1201, 1998a.

Dickey, T. D., G. C. Chang, Y. C. Agrawal, A. J. Williams III, and P. S. Hill, Sediment resuspension in the wakes of Hurricanes Edouard and Hortense, *Geophys. Res. Lett.*, *25*, 3353–3536, 1998b.

Dickey, T. D., et al., Initial results from the Bermuda Testbed Mooring Program, *Deep Sea Res., Part II*, *45*, 771–794, 1998c.

Dickey, T. D., et al., Physical and biogeochemical variability from hours to years at the Bermuda Testbed Mooring Site: June 1994–March 1998, *Deep Sea Res., Part II*, *48*, 2105–2140, 2001.

Donelan, M. A., Air-water exchange processes, in *Physical Processes in Lakes and Oceans*, *Coastal Estuarine Stud.*, vol. 54, edited by J. Imberger, pp 19–36, AGU, Washington, D. C., 1998.

Donelan, M. A., F. W. Dobson, S. D. Smith, and R. J. Anderson, On the dependence of sea surface roughness on wave development, *J. Phys. Oceaongr.*, *23*, 2143–2149, 1993.

Donelan, M. A., F. W. Dobson, S. D. Smith, and R. J. Anderson, Reply to comments on "The dependence of sea surface roughness on wave development," by I. S. Jones and Y. Toba in *J. Phys. Oceanogr.*, *25*, 1905–1907, *J. Phys. Oceanogr.*, *25*, 1908–1909, 1995.

Donelan, M. A., W. M. Drennan, and K. B. Katsaros, The air-sea momentum flux conditions of wind sea and swell, *J. Phys. Oceanogr.*, *27*, 2087–2099, 1997.

Doney, S. C., A synoptic atmospheric surface forcing data set and physical upper ocean model for the U.S. JGOFS Bermuda Atlantic Time-Series Study site, *J. Geophys. Res.*, *101*, 25,615–25,634, 1996.

Doney, S. C., W. G. Large, and F. O. Bryan, Surface ocean fluxes and water-mass transformation rates in the coupled NCAR Climate System Model, *J. Clim.*, *11*, 1420–1441, 1998.

Fofonoff, P., and R. C. Millard, Algorithms for computation of fundamental properties of seawater, *UNESCO Tech. Pap. Mar. Sci. 44*, 53 pp., U. N. Educ. Sci. and Cult. Org., Paris, 1983.

Garratt, J. R., Review of drag coefficients over oceans and continents, *Mon. Weather Rev.*, *105*, 915–929, 1977.

Gill, A. E., On the behavior of internal waves in the wakes of storms, *J. Phys. Oceanogr.*, *14*, 1129–1151, 1984.

Ginis, I., Ocean response to tropical cyclones, in *Global Perspectives on Tropical Cyclones*, edited by R. L. Elsberry, *WMO Tech. Doc. WMO/TD-693*, chap. 5, pp. 198–260, Geneva, Switzerland, 1995.

Greatbatch, R. J., On the response of the ocean to a moving storm: The nonlinear dynamics, *J. Phys. Oceanogr.*, *13*, 357–367, 1983.

Henyey, F. S., J. Wright, and S. M. Flatte, Energy and action flow through the internal wave field: An eikonal approach, *J. Geophys. Res.*, *91*, 8487–8495, 1986.

Herbert, D., and J. N. Moum, Decay of a near-inertial wave, *J. Phys. Oceanogr.*, *24*, 2334–2351, 1994.

Kantha, L. H., and C. A. Clayson, An improved mixed layer model for geophysical applications, *J. Geophys. Res.*, *99*, 25,235–25,266, 1994.

Large, W. G., and G. B. Crawford, Observations and simulations of upper-ocean response to wind events during the Ocean Storms Experiment, *J. Phys. Oceanogr.*, *25*, 2831–2852, 1995.

Large, W. G., and S. Pond, Open ocean momentum flux measurements in moderate to strong winds, *J. Phys. Oceanogr.*, *11*, 324–336, 1981.

Large, W. G., J. C. McWilliams, and P. P. Niiler, Upper ocean thermal response to strong autumnal forcing of the northeast Pacific, *J. Phys. Oceanogr.*, *16*, 1524–1550, 1986.

Large, W. G., J. C. McWilliams, and S. C. Doney, Oceanic vertical mixing: A review and a model with a non-local boundary layer parameterization, *Rev. Geophys.*, *32*, 363–403, 1994.

Large, W. G., J. Morzel, and G. B. Crawford, Accounting for surface wave distortion of the marine wind profile in low-level Ocean Storms wind measurements, *J. Phys. Oceanogr.*, *25*, 2959–2971, 1995.

Levine, M. D., and V. Zervakis, Near-inertial wave propagation into the pycnocline during Ocean Storms: Observations and model comparisons, *J. Phys. Oceanogr.*, *25*, 2890–2908, 1995.

Martin, P. J., Mixed-layer simulation of buoy observations taken during Hurricane Elouise, *J. Geophys. Res.*, *87*, 409–427, 1982.

Martin, P. J., Simulation of the mixed layer at OWS November and Papa with several models, *J. Geophys. Res.*, *90*, 903–916, 1985.

Mellor, G. L., One-dimensional, ocean surface layer modeling, a problem and a solution, *J. Phys. Oceanogr.*, *31*, 790–809, 2001.

Mellor, G. L., and T. Yamada, Development of a turbulence closure model for geophysical fluid problems, *Rev. Geophys.*, *20*, 851–875, 1982.

Michaels, A. F., and A. H. Knap, Overview of the U.S. JGOFS Bermuda Atlantic Time-series Study and the Hydrostation S program, *Deep Sea Res., Part II*, *43*, 157–198, 1996.

Millero, F. J., C. T. Chen, A. Bradshaw, and K. Schleicher, A new high pressure equation of state for seawater, *Deep Sea Res., Part A*, *27*, 255–264, 1980.

Nelson, N. B., The wake of Hurricane Felix, *Int. J. Remote Sens.*, *17*, 2893–2895, 1996.

Pollard, R. T., Properties of near-surface inertial oscillations, *J. Phys. Oceanogr.*, *10*, 385–398, 1970.

Pollard, R. T., and R. C. Millard, Comparison between observed and simulated wind-generated inertial oscillations, *Deep Sea Res.*, *17*, 813–821, 1970.

Price, J. F., Upper ocean response to a hurricane, *J. Phys. Oceanogr.*, *11*, 153–175, 1981.

Price, J. F., Internal wave wake of a moving storm, part I, Scales, energy budget, and observations, *J. Phys. Oceanogr.*, *13*, 949–965, 1983.

Price, J. F., R. A. Weller, and R. Pinkel, Diurnal cycling: observations and models of the upper ocean response to diurnal heating, cooling, and wind mixing, *J. Geophys. Res.*, *91*, 8411–8427, 1986.

Price, J. F., T. B. Sanford, and G. Z. Forristall, Forced stage response to a moving hurricane, *J. Phys. Oceanogr.*, *24*, 233–259, 1994.

Qi, H., R. A. de Szoeke, and C. A. Paulson, The structure of near-inertial waves during Ocean Storms, *J. Phys. Oceanogr.*, *25*, 2853–2871, 1995.

Reed, R. K., On estimating insolation over the ocean, *J. Phys. Oceanogr.*, *7*, 482–485, 1977.

Sanford, T. B., P. G. Black, J. R. Haustein, J. W. Feeney, G. Z. Forristall, and J. F. Price, Ocean response to a hurricane, part I, Observations, *J. Phys. Oceanogr.*, *17*, 2065–2083, 1987.

Shay, L. K., and R. L. Elsberry, Near-inertial ocean current response to Hurricane Frederic, *J. Phys. Oceanogr.*, *17*, 1249–1269, 1987.

Siegel, D. A., et al., Bio-optical modeling of primary production on regional scales: The Bermuda BioOptics Project, *Deep Sea Res., Part II*, *48*, 1865–1896, 2001.

Souza, A. J., T. D. Dickey, and G. C. Chang, Modeling water column structure and suspended particulate matter on the Middle Atlantic continental shelf during the passages of Hurricanes Edouard and Hortense, *J. Mar. Res.*, *59*, 1021–1045, 2001.

Steinberg, D. K., C. A. Carlson, N. R. Bates, R. J. Johnson, A. F. Michaels, and A. H. Knap, Overview of the U.S. JGOFS Bermuda Atlantic Time-

series Study (BATS): A decade-scale look at ocean biology and biogeochemistry, *Deep Sea Res., Part II*, *48*, 1405–1448, 2001.

Taylor, P. K., (Ed.), *Intercomparison and Validation of Ocean-Atmosphere Energy Flux Fields*, 324 pp., WCRP/SCOR Working Group on Air-Sea Fluxes, Geneva, Switzerland, 2000.

Yelland, M., and P. K. Taylor, Wind stress measurements from the open ocean, *J. Phys. Oceanogr.*, *26*, 541–558, 1996.

Yelland, M. J., B. I. Moat, P. K. Taylor, R. W. Pascal, J. Hutchings, and V. C. Cornell, Wind stress measurements from the open ocean corrected for airflow distortion by ship, *J. Phys. Oceanogr.*, *28*, 1511–1526, 1998.

Zedler, S. E., Observations and modeling of the ocean's response to Hurricane Felix at the Bermuda Testbed Mooring (31°44′N, 64°10′W), M. A. thesis, 129 pp., Univ. of Calif. at Santa Barbara, 1999.

Zervakis, V., and M. D. Levine, Near-inertial energy propagation from the mixed layer: Theoretical considerations, *J. Phys. Oceanogr.*, *25*, 2872–2889, 1995.

T. D. Dickey, X. Yu, and S. E. Zedler, Ocean Physics Laboratory, University of Cailfornia, Santa Barbara, Santa Barbara, CA 93106, USA.

S. C. Doney, National Center for Atmospheric Research, Boulder, CO 80305, USA.

G. L. Mellor, Princeton University, Princeton, NJ 08544, USA.

J. F. Price, Woods Hole Oceanographic Institution, Woods Hole, MA 02543, USA.